AD-A102 241 NIELSEN ENGINEERING AND RESEARCH INC MOUNTAIN VIEW CA F/G 20/4
BASIC STUDIES OF BODY VORTICES AT HIGH ANGLES OF ATTACK AND SUP--ETC(U)
OCT 80 G H KLOPFER, J N NIELSEN N00014-78-C-0490
UNCLASSIFIED NEAR-TR-226 NL

1 OF 1
AD A
102241

END
DATE
FILMED
8-81
DTIC

LEVEL II

(12)

NIELSEN ENGINEERING
AND RESEARCH, INC.

OFFICES: 510 CLYDE AVENUE / MOUNTAIN VIEW, CALIFORNIA 94043 / TELEPHONE (415) 968-9457

COPY NO. 13

BASIC STUDIES OF BODY VORTICES AT HIGH ANGLES OF ATTACK AND SUPERSONIC SPEEDS

by

Goetz H. Klopfer and Jack N. Nielsen

NEAR TR 226

October 1980

Final Report

For the period 1 June 1979 to 31 May 1980

Prepared under Contract No. N00014-78-C-0490

for

OFFICE OF NAVAL RESEARCH
Arlington, Virginia 22217

by

NIELSEN ENGINEERING & RESEARCH, INC.
510 Clyde Avenue, Mountain View, CA 94043
Telephone (415) 968-9457

Pages 4 and 6 are intentionally left blank

Change of Address

Organizations receiving reports on the initial distribution list should confirm correct address. This list is located at the end of the report. Any change of address or distribution should be conveyed to the Office of Naval Research, Code 211, Arlington, VA 22217.

Disposition

When this report is no longer needed, it may be transmitted to other organizations. Do not return it to the originator or the monitoring office.

Disclaimer

The findings and conclusions contained in this report are not to be construed as an official Department of Defense or Military Department position unless so designated by other official documents.

Reproduction

Unclassified

SECURITY CLASSIFICATION OF THIS PAGE (When Data Entered)

REPORT DOCUMENTATION PAGE		READ INSTRUCTIONS BEFORE COMPLETING FORM
1. REPORT NUMBER	2. GOVT ACCESSION NO. AD-A102241	3. RECIPIENT'S CATALOG NUMBER
4. TITLE (and Subtitle) Basic Studies of Body Vortices at High Angles of Attack and Supersonic Speeds		5. TYPE OF REPORT & PERIOD COVERED Final Report. 6/1/79 - 5/31/80
		6. PERFORMING ORG. REPORT NUMBER NEAR-TR-226
7. AUTHOR(s) Goetz H. Klopfer [redacted] Jack N. Nielsen		8. CONTRACT OR GRANT NUMBER(s) N00014-78-C-0490
9. PERFORMING ORGANIZATION NAME AND ADDRESS Nielsen Engineering & Research, Inc. 510 Clyde Avenue Mountain View, CA 94043		10. PROGRAM ELEMENT, PROJECT, TASK AREA & WORK UNIT NUMBERS 61153N RR 014 11 04 NR 061-272
11. CONTROLLING OFFICE NAME AND ADDRESS Office of Naval Research Arlington, Virginia 22217		12. REPORT DATE October 1980
		13. NUMBER OF PAGES 85
14. MONITORING AGENCY NAME & ADDRESS (if different from Controlling Office) RR01411		15. SECURITY CLASS. (of this report) Unclassified
		15a. DECLASSIFICATION/DOWNGRADING SCHEDULE

16. DISTRIBUTION STATEMENT (of this Report)

Approved for public release; distribution unlimited.

17. DISTRIBUTION STATEMENT (of the abstract entered in Block 20, if different from Report)

18. SUPPLEMENTARY NOTES

19. KEY WORDS (Continue on reverse side if necessary and identify by block number)

Numerical Analysis
Supersonic Flows
Euler Equations
High Angle of Attack Aerodynamics
Body Vortices

20. ABSTRACT (Continue on reverse side if necessary and identify by block number)

The problem of computing the steady inviscid supersonic flows about tangent ogive cylinders at high angles of attack with symmetric body vortices is solved in this report.

To obtain an efficient procedure the steady Euler equations are used as the basic governing equations as opposed to the more complicated Navier-Stokes equation. The viscous effects, important near the separation line, are simulated by a Kutta

DD FORM 1 JAN 73 1473 EDITION OF 1 NOV 65 IS OBSOLETE

Unclassified

SECURITY CLASSIFICATION OF THIS PAGE (When Data Entered)

384752

Block 20 (Continued)

condition. The rest of the flow field is essentially controlled by the inviscid equations. The equations, written in conservation form in generalized curvilinear coordinates, are approximated by MacCormack's second-order accurate predictor-corrector algorithm. The flow tangency conditions at the body surface are satisfied by Abbett's scheme and the outer bow-shock position by the Rankine-Hugoniot jump relations. Internal shock waves or tangentially discontinuities are captured.

Comparisons have been made between the present theory and experimental data for 2.0 and 3.0 caliber tangent ogive nose lengths at $\alpha = 15°$ and $20°$ and $M_\infty = 3.0$. Good agreement is obtained. Results were also obtained for a 5.0 caliber tangent ogive nose length configuration for comparison with a numerical solution obtained by solving the Navier-Stokes equation and with experimental data.

SUMMARY

This paper addresses the problem of computing the steady inviscid supersonic flows about tangent ogive cylinders at high angles of attack. For such cases the flow on the leeward side tends to separate and spiral into symmetric vortices. At higher angles of attack asymmetric vortex separation can occur. In this report only the symmetric cases are considered.

Previous analytical studies to solve these flow fields have used the vortex-cloud method of Mendenhall. This method is basically inviscid and semi-empirical. Viscous effects have been included by Pulliam in a numerical study of transonic flows over hemisphere cylinders and supersonic flows over tangent ogive cylinders. These studies were based on the Navier-Stokes equations, the former on the time-dependent three dimensional Navier-Stokes equations and the latter on the parabolized Navier-Stokes equations. To obtain a more efficient procedure we use the steady Euler equations as the basic governing equations as opposed to the more complicated Navier-Stokes equation. The viscous effects, important near the separation lines, are simulated by a Kutta condition. The separation lines are determined from experimental data. The rest of the flow field is essentially controlled by the inviscid equations. The equations are written in conservation form in generalized curvilinear coordinates. The equations are approximated by MacCormack's second-order accurate predictor-corrector algorithm. The flow tangency conditions at the body surface are satisfied by Abbett's scheme and the outer bow-shock position by the Rankine-Hugoniot jump relations. Any internal shock waves or tangentially discontinuities are captures by the scheme.

Comparisons are made between the results based on the present procedure and experimental data for 2.0 and 3.0 caliber tangent-ogive noses on a cylindrical body at $\alpha = 15°$ and $20°$ and

a free-stream Mach number $M_\infty = 3.0$. Good agreement is obtained in predicting the flow field and the vorticity in the recirculating region. Results are also obtained for a 5.0 caliber-long tangent ogive nose configuration for comparison with a numerical solution based on the parabolized Navier-Stokes equation and with experimental data. These results indicate that the present procedure gives much better agreement with experimental data than the Navier-Stokes equation results.

PREFACE

The authors would like to express their appreciation to Dr. Tom Pulliam of NASA/Ames Research Center for providing some numerical data, and to Dr. Lewis Schiff also of NASA/Ames for his kind help.

This technical report covers the work performed under Contract N00014-78-C-0490 from 1 June 1979 to 31 May 1980. The program is sponsored by the Office of Naval Research, Arlington, Virginia. Mr. Robert von Husen was the Scientific Officer.

TABLE OF CONTENTS

1. INTRODUCTION

As a result of past work (refs. 1 and 2) done at Nielsen Engineering & Research, Inc. (NEAR) for the Office of Naval Research (ONR) to produce engineering prediction methods for missiles up to angle of attack of 50° and Mach numbers up to 3.0, several important problems in high angle of attack aerodynamics have emerged. It is the purpose of this report to describe these problems and to attempt their solution using the Euler equations. While these problems have arisen in connection with missile aerodynamics, they are equally important for airplanes.

The present work is a logical extension of the work NEAR has carried out for ONR over the past five years. During the first two years, paneling (inviscid) methods together with vortex theory were used to develop pressure predictive techniques for complete missiles at supersonic speeds and angles of attack to 20°. In the third and fourth years engineering methods were developed to predict forces and moments acting on canard cruciform missiles to 50° angle of attack. These methods, based on data base and rational modeling, produced useful methods of reasonable accuracy, but also uncovered important aerodynamic effects which need more basic study in their own right. In order to extend the range of the engineering design codes and to improve the rational modeling approach, it is necessary to undertake further work. It is believed that such work should utilize recent advances in viscous and inviscid numerical computation techniques supplemented by further experimental work.

Two of the major problems which have been uncovered are the adverse effect of wing-body interference on wing lift at high angles of attack and the special behavior of body vortices at supercritical crossflow Mach numbers. The former problem was

covered in last year's contract (ref. 3). This report addresses the latter problem only.

We will first discuss the background of vortex shedding from bodies from the physical point of view so that the significance of the present work can be brought into focus. Next the state of the analytical art is reviewed as it bears on the problem. Then the means of introducing compressibility into the problem is discussed. This means is the same as that used for last year's contract, namely, solving the steady Euler equations of motion numerically. The viscous effects are simulated by imposing a Kutta condition where the flow is to separate from the body. The numerical procedure will not be described here as it has been already described in the previous year's final report (ref. 3). Changes from the previous method will be pointed out however. The report concludes with a section on a comparison of the present numerical results with experimental data (refs. 4, 5, 6, and 7) and a Navier-Stokes solution obtained by an implicit numerical scheme developed at NASA/Ames (ref. 18).

2. BACKGROUND

2.1 Vortex Separation for Subcritical Crossflow

The shedding of vortices from a body of revolution at angle of attack has a number of regimes. If the crossflow Mach number is less than about 0.5, the crossflow is subcritical, and several types of steady vortex patterns can exist on the leeward side of the body depending on its fineness ratio and its angle of attack. The two types of vortex shedding are characterized as symmetric and asymmetric as shown in Figure 1. The boundary between symmetric and asymmetric vortex shedding for subcritical crossflow has been extensively studied by a number of investigators, and a good summary of the state of art is given by Chapman, Keener, and Malcolm in reference 9. For pointed bodies of

revolution, these authors show that asymmetry starts at an angle of attack of about twice the nose semi-apex angle. For a conical nose of total angle 25°, asymmetry might occur at about $\alpha = 25°$. For an L/D = 3.5 tangent ogive nose, asymmetry starts at about 32°.

2.2 Vortex Separation for Supercritical Crossflow

If the crossflow Mach number ($M_\infty \sin \alpha$) is much greater than about 0.5, the crossflow is said to be supercritical. In this case the nature of the vortex separation from the body is of a totally different type from those shown in Figure 1. Consider Figure 2 in which the shock waves are not all shown. Asymmetric vortices do not now appear (ref. 9). Instead two elongated elliptic-like regions of distributed vorticity form on each side of the body as shown. The boundary layer separates on both sides of the body and feeds into the elongated vorticity regions. As the angle of attack increases, the height of the vorticity region increases as shown in Figure 3 (ref. 2).

In addition to these features, vapor screen photographs sometimes show what appears to be a horizontal shock between the regions of vorticity. Also there appear to issue from between the tops of the regions weak alternating vortices.

2.3 Regions of Various Vortex Separation Types

Let us now examine the $\alpha - M_\infty$ diagram in Figure 4 which shows the regions where the foregoing three classes of vortex formations prevail. If $M_C = 0.5$ is the boundary between the subcritical and supercritical case, then above the boundary we have symmetric elliptical vorticity regions. Below the boundary, we have two regions separated by the α = constant line between symmetric and asymmetric separation. What this figure shows is

that the supercritical case occupies a large part of the high angle of attack region over the Mach number range, and is thus of considerable importance. The boundaries as given in this figure are based on approximate rules of thumb, but the general conclusion is not changed thereby. Another point that needs to be made is that under the $M_c = 0.5$ boundary, the symmetric vortex model is significantly influenced by compressibility for supersonic Mach numbers. It is the effect of compressibility on the vortex pattern that we desire to predict, particularly that for supercritical crossflow. No method for studying this problem exists except possibly computer programs based on the unsteady three-dimensional Navier-Stokes or the parabolized Navier-Stokes equations (refs. 8 and 10). These codes require very long computer runs.

2.4 Technical Approach

The originally envisaged technical approach was to combine the vortex-cloud method of Mendenhall (refs. 11 and 12) with the shock-capturing Euler code described in reference 3. The vortex-cloud methodology has presently been developed for incompressible flow, and the flow is governed by the Laplace equation. The vortices are introduced into the flow as point vortices which also satisfy the Laplace equation. Linear superposition is used. In the case of compressibility, the general flow is governed by the Euler equations which permit compressibility and shock waves. The Euler equations also permit distributed vorticity throughout the field as long as the flow is inviscid. This means that the vorticity is convected but not diffused by molecular action. This assumption should be quite good. We now discuss the vortex-cloud method for incompressible flow and then describe the necessary modifications and complications for compressible flow.

2.4.1 Incompressible Vortex-Cloud Method.- In the vortex-cloud method an analogy is made between three-dimensional steady

flow about a body and two-dimensional unsteady flow about a circle. Perhaps a good way to envision this analogy is to consider plane AA in Figure 2. Let the plane remain fixed and let the body pierce the plane at time $t = 0$. At this point there is no flow in the plane. After it has penetrated the plane a certain distance, it will have a separated vortex flow pattern. The pattern shown in Figure 2 is for a supercritical case, but for a subcritical case the calculated crossflow discrete vortex pattern would appear as in Figure 5 for symmetric vortices and as in Figure 6 for asymmetric vortices.

The way in which such vortex clouds are calculated is now described. As the body of revolution at some angle of attack passes through plane AA, the pressure distribution around its circumference in this plane is calculated, and the lower stagnation point in the crossflow plane located. From this pressure distribution it is possible to determine the location of the separation points using the Stratford criterion (assuming separation exists). Separation usually starts at the top of the body for symmetric flows. At the separation points vortices are introduced into the flow to represent the vorticity of the separated boundary layer. This vorticity flux per unit time is $d\Gamma/dt$ given by

$$\frac{d\Gamma}{dt} = \frac{1}{2} \frac{U_\delta^2}{2} (\Lambda)$$

Here U_δ is the crossflow velocity at the edge of the boundary layer as given by the flow solution including any upstream vortex effects. The factor Λ is an experimental factor equal to about 0.6 to account for vorticity of opposite sign feeding into the separation point from above. A figure illustrating these points is shown as Figure 7. By tracking the vortices downstream and applying the method to a series of crossflow planes, the entire vortex cloud can be calculated. It is noted that any upstream

effects of the vortex cloud in influencing the pressures is not included. This is an approximation of the two-dimensional analogy.

2.4.2 Vortex-Cloud Method for Compressible Flows.- The incompressible method must be modified for compressibility in several ways.

1. Determine pressure distribution using Euler equations.
2. Account for compressibility on separation position.
3. Introduce compressible analog of incompressible vortices into the method.

With regard to the first point, it is of interest to examine Figure 8 which shows the flow in the crossflow planes of a body of revolution in supercritical crossflow without vortices. It is noted that crossflow shocks going to the body surface exist in the crossflow plane. It is clear that significant compressibility effects occur on the separation locations.

With regard to the position of separation, it is clear from the foregoing example that new considerations have arisen. As the boundary layer moves around the body from the bottom, it crosses the M = 1 line and accelerates into the imbedded supersonic region. Whether it starts a recompression before reaching the shock is not clear, but at any rate the separation mechanism may be the shock. In this case a different separation criterion than that of Stratford may be required. Also the flux of vorticity shed by the separating boundary layer will probably be different. Some theoretical means of handling this local shock-wave, boundary-layer interaction will probably be required. It may possibly be obtained from existing shock-wave boundary-layer interaction methods.

The third question of introducing a vortex element into the flow to represent the vorticity flux of the boundary layer is not

a simple one aside from the problem of superpositioning. We cannot just introduce point vortices of the incompressible type with images inside the cylinder. Since we are calculating a vortical field with a separation streamline emanating from the surface, a crossflow separation point will be required. This change will introduce the desired flux into the flow field at the separation point.

In this investigation we will consider the case for which the Mach number parallel to the body axis is supersonic so that we can use a marching procedure for the Euler codes. Otherwise an extensive interaction procedure will be required using much computer time. This case will also avoid the shortcomings of the incompressible vortex-cloud method in not accounting for the upstream influences of the vortex cloud.

It is also clear that once we can determine the vortical flow using Euler equation methods, we can add a wing and determine the interference of the body vortices on the wing. This is the link between the previous work on wing-body interference without forebody vortices and the present work.

A brief outline of the general approach of studying the body vortex problem for steady supersonic flows is now given.

The steady Euler equations are written in conservation form in generalized curvilinear coordinates. The general coordinate system is fitted between the body and the outer bow shock. The coordinate system is fitted to the body by a conformal transformation which transforms the body to a unit circle. To fit the outer shock to the coordinate system, the radial distance is normalized with respect to the distance between the outer shock and the body. A typical mesh is shown in Figure 9 for a tangent ogive cylinder body. The equations are approximated by MacCormack's second-order accurate predictor-corrector algorithm (refs. 13 and 14). The flow tangency conditions at the body surface are satisfied by Abbett's scheme (ref. 15) and the outer

bow-shock position by the Rankine-Hugoniot jump relations. Any internal shock waves and tangential discontinuities or vortex sheets are captured by the scheme. Separated flow on the body will be enforced by a Kutta condition imposed at empirically determined separation lines.

In the following section the governing transformed equations will be discussed. Although these equations were covered by the previous final report (ref. 3), certain changes have been made and it is worthwhile to repeat these equations here for completeness. The description of the proper Kutta condition applied on smooth bodies follows. The final two sections will cover the numerical results and the conclusion and recommendations. The description of the numerical scheme, boundary and initial conditions, and body geometry will not be covered in this report. These have been adequately covered by the previous report (ref. 3).

3. STEADY EULER EQUATIONS

The conservation-law form of the fluid dynamic equation for steady, inviscid, three-dimensional compressible flow of an ideal gas (steady Euler equations) in Cartesian form are

$$\frac{\partial \hat{E}}{\partial x} + \frac{\partial \hat{F}}{\partial y} + \frac{\partial \hat{G}}{\partial z} = 0 \tag{1}$$

where $\hat{E}$, $\hat{F}$, and $\hat{G}$ are defined as

$$\hat{E} = \begin{bmatrix} \rho u \\ \rho u^2 + kp \\ \rho uv \\ \rho uw \end{bmatrix} \qquad \hat{F} = \begin{bmatrix} \rho v \\ \rho uv \\ \rho v^2 + kp \\ \rho vw \end{bmatrix} \qquad \hat{G} = \begin{bmatrix} \rho w \\ \rho uw \\ \rho vw \\ \rho w^2 + pk \end{bmatrix}$$

Equation (1) represents the conservation of mass and momentum. The pressure and density are normalized with respect to the stagnation conditions and the Cartesian velocity components (u,v,w) with respect to the maximum adiabatic velocity where $k = 2\gamma/(\gamma-1)$ and γ is the ratio of the specific heats. The system of equations is closed by the integrated form of the steady energy equation which in nondimensional form is

$$p = \rho(1 - u^2 - v^2 - w^2) \tag{2}$$

For a given free-stream Mach number and angle of attack α, the remaining free-stream variables in nondimensional form are given by

$$p_\infty = \{1 + [(\gamma-1)/2]M_\infty^2\}^{-\gamma/(\gamma-1)}$$

$$\rho_\infty = \{1 + [(\gamma-1)/2]M_\infty^2\}^{-1/(\gamma-1)}$$

$$u_\infty = 0$$

$$v_\infty = q_\infty \sin\alpha$$

$$w_\infty = q_\infty \cos\alpha$$

where

$$q_\infty = (u_\infty^2 + v_\infty^2 + w_\infty^2)^{1/2} = \left(\frac{\frac{\gamma-1}{2}M_\infty^2}{1 + \frac{\gamma-1}{2}M_\infty^2}\right)^{1/2}$$

To obtain a surface-oriented coordinate system, the system (1) is transformed from the Cartesian space (x,y,z) into another arbitrary curvilinear system (z,r,ϕ) where r = 1 defines the body surface. The general transformation is (the particular transformations considered are given in section 3 of reference 3).

$$
\begin{aligned}
z &= z \\
r &= r(x,y,z) \\
\phi &= \phi(x,y,z)
\end{aligned}
\tag{3}
$$

The transformed equations, obtained by Viviand's procedure (described in ref. 3), are in slightly rearranged form

$$\frac{\partial}{\partial z}\tilde{E} + \frac{\partial}{\partial r}\tilde{F} + \frac{\partial}{\partial \phi}\tilde{G} = 0 \tag{4}$$

where

$$\tilde{E} = \frac{1}{J}\begin{bmatrix} \rho U \\ \rho wU + pk \\ \rho vU \\ \rho uU \end{bmatrix} \quad \tilde{F} = \frac{1}{J}\begin{bmatrix} \rho V \\ \rho wV + r_z pk \\ \rho vV + r_y pk \\ \rho uV + r_x pk \end{bmatrix} \quad \tilde{G} = \frac{1}{J}\begin{bmatrix} \rho W \\ \rho wW + \phi_z pk \\ \rho vW + \phi_y pk \\ \rho uW + \phi_x pk \end{bmatrix}$$

and

$$
\begin{aligned}
U &= w \\
V &= r_x u + r_y v + r_z w \\
W &= \phi_x u + \phi_y v + \phi_z w
\end{aligned}
\tag{5}
$$

where U, V, and W are the contravariant velocities written without the metric normalization. The metric terms are obtained from the chain rule expansion of x_r, y_r, etc. and solved for r_x, r_y, etc. to give

$$
\begin{aligned}
z_x &= 0 \qquad & r_x &= Jy_\phi \qquad & \phi_x &= -Jy_r \\
z_y &= 0 \qquad & r_y &= -Jx_\phi \qquad & \phi_y &= Jx_r \\
z_z &= 1 \qquad & r_z &= J(y_z x_\phi - x_z y_\phi) \qquad & \phi_z &= J(x_z y_r - x_r y_z)
\end{aligned}
\tag{6}
$$

and

$$J^{-1} = x_r y_\phi - x_\phi y_r$$

where J is the Jacobian of the transformation from the arbitrary curvilinear space (z,r,ϕ) to the Cartesian space (x,y,z), Figure 10. It should be pointed out that both coordinate systems are left-handed, the reason being that the parent code (refs. 13 and 14) used for this study was written for a left-handed system.

To fit the outer bow shock wave, the outer mesh boundary must coincide with the bow shock. Since this bow shock is a variable three-dimensional surface it is necessary to introduce another transformation which normalizes the distance between the body boundary and the bow shock surface. The location of the bow shock surface is determined by the Rankine-Hugoniot conditions during the course of the numerical computation described in a later section. At the same time it is desirable to have arbitrary clustering functions in the transformation so that mesh points can be concentrated near the body surface, wing tip, or wing-body juncture for increased resolution in areas of rapid changes of the flow variables or the previously mentioned transformation metrics.

The equations of the independent variable transformation are

$$\begin{aligned} \zeta &= z \\ \tau &= h(\xi) \\ \eta &= f(\phi) \end{aligned} \tag{7}$$

where h and f are clustering functions. The radial variable, ξ, is

$$\xi = (r - r_b)/(r_s - r_b)$$

where $r_b = r_b(z,\phi)$, the body surface radius

and

$r_s = r_s(z,\phi)$, the outer shock radius

are to be determined as part of the numerical solution procedure. The system (1) may now again be written in strongly conservative

form

$$\frac{\partial}{\partial \zeta} E + \frac{\partial}{\partial \tau} F + \frac{\partial}{\partial \eta} G = 0$$

where

$$E = \tilde{E}/\mathcal{D}$$

$$F = \tau_\xi \{\xi_z \tilde{E} + \xi_r \tilde{F} + \xi_\phi \tilde{G}\}/\mathcal{D}$$

$$G = \eta_\phi \tilde{G}/\mathcal{D}$$

and

$$\mathcal{D} = \tau_\xi \xi_r \eta_\phi$$

We also have

$$\tau_\xi = \frac{dh(\xi)}{d\xi}$$

$$\xi_r = 1/(r_s - r_b)$$

$$\xi_z = -\{r_{bz} + \xi(r_{sz} - r_{bz})\} \cdot \xi_r$$

$$\xi_\phi = -\{r_{b\phi} + \xi(r_{s\phi} - r_{b\phi})\} \cdot \xi_r$$

$$\eta_\phi = \frac{df(\phi)}{d\phi}$$

The functions h and f are the clustering transformations in the r and ϕ directions, respectively. The normalization between the body surface and the shock is given by the variable ξ.

The equation is still in strongly conservative form unlike in reference 3 where it was thought that the weakly conservative form is necessary to simplify the decoding of the dependent E vector. The finite difference form of equation (4) is integrated with respect to the hyperbolic coordinate ζ to yield values of E. The physical flow variables p, ρ, u, v, w must be decoded from the components e_i of E. Explicit expressions are possible for the physical flow variables even if the system is strongly conservative. The decoding procedure has been described in

reference 3 and is identical as required for this equation set if J is replaced by $J\mathcal{D}$.

4. KUTTA CONDITION AND BOUNDARY CONDITIONS

Several types of boundary conditions must be satisfied for the problem considered in this report. These include solid surfaces such as the body surface, permeable surfaces such as the fitted outer bow shock wave, symmetry planes, and initial planes from which the computation can be started. Another type of boundary considered is at points on the body where the flow separates. At these locations the flow tangency condition is not adequate. The separate procedure devised to obtain the flow variables at these points is described below. The other conditions are essentially the same as discussed in reference 3 and will not be repeated here.

In the previous study (ref. 3) separated flows over wing-body combinations were considered. The wings were assumed to be thin and planar. For these types of wings with their sharp leading edges, the separation line is known a priori, namely at the sharp leading edges. Furthermore it was shown previously that at the sharp leading edges the transformation metrics and Jacobian vanish. Thus arbitrary values of the flow variables will satisfy the Euler equation since these equations are indeterminate at the leading edges. However, for the tangent ogive cylinders considered in this report, the separation line is not known a priori. Neither do the Euler equations become indeterminate anywhere on the body. Thus a different type of Kutta condition must be prescribed for these types of bodies.

The specification of the Kutta condition to enforce separated flow is straightforward. The five flow variables must be specified. They are the three Cartesian velocity components,

u, v, w and the pressure and density. The values of these five variables are not arbitrary as in the previous study (ref. 3) since the transformed equations are not indeterminate. This means that the flow variables must satisfy the continuity, momentum, and energy equations. Since we want to force separation, the flow variables must satisfy the conditions for a tangential discontinuity. The conditions for a tangential discontinuity surface or vortex sheet are

a) p is continuous across the sheet

b) the velocity normal to the sheet is zero

c) total enthalpy is constant

d) the jump in the velocity tangential to the sheet is arbitrary

e) the jump in the density ρ across the sheet is arbitrary

The jump relations state that the jumps in density and tangential velocity are arbitrary. This means that the jumps are not determined by the local conditions, but by global conditions. The global conditions are determined by the governing equations and boundary conditions and not the jump relations.

The vortex sheet coming off the body is shown in Figure 11. Two geometric parameters determine the location and orientation of this sheet. They are ϕ_s and ϕ_c for the location and orientation, respectively, as shown in Figure 11. On each side of this vortex sheet, separate values of p, ρ, u, v, w must be prescribed. However, since this sheet is to be captured by the finite difference scheme it is more appropriate to prescribe some mean values of p, ρ, u, v, w within the sheet. These mean values will be some weighted average of the values on either side of the sheet. Thus we can prescribe some mean velocity vector within the sheet

by q_o (Fig. 11). This is the mean tangential velocity vector oriented by angle ϕ_a from the axial direction (z-coordinate).

The conditions for separation at a point on the body $\phi = \phi_s$ are implemented as follows, with reference to Figure 12:

a) $p_o = 0.5(p_1 + p_{-1})$

b) $\rho_o = 0.5(\rho_1 + \rho_{-1})$

c) total enthalpy is constant

where the subscript "o" designates the separation point, "1" the first point on the body on the leeside of the vortex sheet, and "-1" the first point on the body on the windward side. In other words, the pressure and density at the separation point are obtained by averaging over the nearest surface neighboring values. These three conditions are sufficient to determine the mean tangential velocity q_o in the vortex sheet as shown in Figures 11 and 12. To obtain the Cartesian velocity components u_o, v_o, and w_o, the three geometric parameters ϕ_s, ϕ_c, and ϕ_a are required. Since the Euler equations do not account for the viscous effects, which control the separation, additional information is required to determine the three geometric parameters. These parameters will be determined from empirical data for the present study. The three velocity components at the separation point are given by

$$w_o = q_o \cos \phi_a$$

$$u_o = q_o \sin \phi_a \cos(\phi_s - \phi_c)$$

$$v_o = q_o \sin \phi_a \sin(\phi_s - \phi_c)$$

The above procedure has been used successfully in computing separated flow over smooth bodies. However, it may be possible to improve the procedure. For example, condition (a) simply averages the pressure over its nearest neighbors. Some experimental data seem to indicate, though, that the pressure reaches a local extremum at the crossflow separation points. This can be

seen in Figure 13 (Peake and Tobak, ref. 16), which shows the location of the separation points by an oil film and the corresponding pressure in the crossflow plane. A simple pressure averaging would thus underpredict the pressure at the separation point. A more accurate method would be to extrapolate the pressures to the separation point from each side and then average. This has not been tried in this study.

It would also be useful to obtain the three geometric parameters from some sort of separation criteria such as the Stratford criteria which works well for subsonic flows. If a compressible separation criteria can be established, then the Euler code can be used to determine separated flows independently of any particular set of empirical data.

5. NUMERICAL RESULTS

In this section some of the numerical results obtained by the Euler code with a Kutta condition will be covered. Two cases are discussed. Firstly, a two-caliber tangent-ogive cylinder at a free-stream Mach number of 3.0 and angle of attack (α) of 15° is presented. This will give a direct comparison to the experimental data of Oberkampf (ref. 6) and to the vortex-cloud method of Mendenhall (ref. 17). Secondly, a five-caliber tangent-ogive cylinder at $M_\infty = 2.9$ and $\alpha = 20°$ is computed. This case will allow comparison with results obtained by a parabolized Navier-Stokes code by Pulliam (ref. 18). A parametric study of the geometric parameters required for the Kutta condition is also carried out. These results will be presented first.

5.1 Geometric Parametric Study

A parametric study of the three geometric parameters ϕ_s, ϕ_c, and ϕ_a is required to complete the specification of the Kutta

condition. This will determine the relative importance of each of the parameters in controlling the size of the separated flow region and the amount of vorticity shed into this region. This study was carried out on a three-caliber tangent-ogive nose with a cylindrical afterbody at $M_\infty = 3.0$ and $\alpha = 20°$. A simple way of determining the relative effects of the parameters is to perturb each of the parameters around a base combination of $\phi_s = 90°$, $\phi_c = 30°$, and $\phi_a = 10°$. The base combination values were estimated from experimental data such as those shown in Figure 13 (obtained from ref. 16).

The results indicate that the most influential parameter is the separation angle, ϕ_s. This parameter determines the location of the separation vortex sheet on the body. As shown in Figure 14(a), the separation angle has a significant effect on both the total amount of vorticity shed into the separated region and on the height of this region as measured on the leeward plane of symmetry. The crossflow angle, ϕ_c, seems to have very little effect on the rate of vorticity shedding, Figure 14(b). Both the vertical height of the leeward plane stagnation point and the total circulation are essentially independent of this parameter. The axial angle ϕ_a has a rather moderate effect on the vorticity shedding rate and a somewhat stronger effect on the height; Figure 14(c).

The results indicate that the major influential geometric parameter is the separation angle ϕ_s. The axial angle parameter is of only moderate importance and the crossflow angle ϕ_c seems to have virtually no influence. This means that if the parameters are to be determined empirically, the most accuracy required is on ϕ_s and rough estimates are sufficient for the remaining two. This is fortuitous since the separation angle can be accurately determined from oil flow or vapor screen data. However, it is more difficult to determine the axial angle ϕ_a and the crossflow angle ϕ_c.

5.2 Pressure Interpolation

As mentioned in section 4 the pressure at the separation line is determined by linear interpolation from the nearest neighboring points on the body. It is not clear that this is the best strategy. Although the pressure is constant across a vortex sheet, there may be strong pressure gradient leading up to the separation line as indicated by Peake and Tobak (ref. 16) and shown in Figure 13. If the mesh spacing is fine enough near the separation line, then linear interpolation should be adequate. Some pressure data are available from reference 7 with which direct comparisons can be made for the numerical calculation using the base values of the geometric parameters of the previous section. These comparisons are given in Figures 15a through 15c for three different axial stations. Shown are the circumferential pressure distributions for a 3.0-caliber tangent-ogive nose with a cylindrical afterbody at $\alpha = 20°$ and $M_\infty = 2.96$ for the experimental data and $M_\infty = 3.00$ for the numerical results. The agreement is reasonable except at the windward crossflow stagnation point ($\phi = 0°$) and over the separated region. There are probably two reasons for this discrepancy. The numerical results have the Kutta condition imposed at $\phi = 90°$ which is the approximately asymptotic value of the experimental separation line. The experimental separation line varies as shown in Figure 16 from $\phi = 160°$ at $z/D = 2.0$ to $\phi_s = 90°$ at $z/D = 80$. This separation line is determined from the oil flow data shown in Figure 17. The asymptotic value at $z/D \geq 8$ is determined from similar data from Peake and Tobak (ref. 16). Thus the separation occurs at different circumferential locations and the discrepancies are to be expected. The other reason is probably the lack of accuracy in determining the axial angle, ϕ_a. While this parameter has only a moderate effect on the overall flow separation, i.e. size and vortex shedding rate, it seems to have a much stronger effect on the local pressure distribution. This can be

seen in Figure 15 as a large oscillation in the pressure near the imposed separation point ($\phi_s = 90°$) for an axial angle $\phi_a = 10°$. This case was rerun with a variable separation line given in Figure 16 from the oil flow data of Figure 17. With the axial angle varying from 0° at z/D = 2.0 to only 5° at z/D = 8.0 the results shown in Figures 18a and b were obtained. The large oscillations are nearly absent but agreement with the experimental data is not notably improved in the separated region. There may be two or more separation lines. Unfortunately the experimental pressure data resolution is rather coarse (every 22.5° circumferentially) for this case. Thus it is not possible to discern the additional separation lines. The oil flow data are also not clear enough to determine these. Although the pressure comparisons may be suspect, the overall flow field prediction is good such as the location of the outer bow shock and the overall size and shape of the separated region. This may be seen in Figure 19, which shows the numerical results superimposed on the experimental data. It is somewhat difficult to discern the size of separated zone from the schlieren and vapor-screen photographs. For this reason another set of runs was made for a 2.0-caliber tangent-ogive cylinder for which detailed flow field data are available.

5.3 Numerical Results

Other numerical results have been obtained for two tangent ogive circular bodies at two angles of attack and free-stream Mach numbers. The first case for which there exist extensive experimental flow field data within the separated region is for a 2.0 caliber tangent-ogive nose and cylinder combination at Mach 3.0 and angle of attack of 15°. The second case is a 5.0 caliber tangent-ogive nose and cylinder combination at $M_\infty = 2.9$ and $\alpha = 20°$. For this latter case an independent numerical calculation based on the parabolized Navier-Stokes equation

(ref. 18) is available. For both of these cases the Kutta condition is started at $z/D = 2.0$ and the separation angle ϕ_s is kept constant at 90°. The vortex orientation angle, ϕ_c, and the axial angle, ϕ_a, are 30° and 10°, respectively.

5.3.1 Two Caliber Tangent Ogive Cylinder.- For this configuration direct comparison may be made with the extensive experimental data of Oberkampf (refs. 4, 5, and 6). These data cover only the flow field; surface data such as circumferential pressure distribution and oil flow data are not available. The first numerical result presented are the crossflow velocity vectors at a station thirteen calibers downstream of the nose tip, Figure 20. Only the leeward quadrant is shown. As can be seen from the figure, separation occurs at $\phi = 90°$ and the entire lee side of the body is in the reversed flow field. No allowance was made for a possible secondary separation. Other experimental data (Peake and Tobak, ref. 16) indicate that for this Mach number, angle of attack and configuration, secondary separation occurs. Also indicated in this figure is the approximate location of the vortex center and the height (by y_{stag}) of the separated flow region. The heavy dotted line outlines the area covered by Oberkampf's data in Figure 21. The experimental vortex center is somewhat smeared out but overlaps the predicted location. The extent of the separated region is predicted within 3 percent of the body diameters. Unfortunately the surface data are not available for determining the primary or secondary separation point. The axial growth of the circulation around the contour shown in Figure 20 by the heavy dotted line, plane of symmetry, body, and $\phi = 90°$ is shown in Figure 22. The agreement with Oberkampf's data is good. Also shown are the results obtained by the vortex-cloud theory of Mendenhall (ref. 17). It consistently underpredicts the circulation for this Mach number.

The crossflow particle paths of the numerical prediction are depicted in Figure 23. This plot shows the flow field as would

be seen by a vapor-screen visualization. There is a spurious vortex just behind the separation line which is due to the large surface pressure oscillation. The main vortex is typically of those observed experimentally, i.e. elongated and elliptical in shape. It is possible that the spurious vortex indicate that the numerical results should have allowed for a secondary separation.

While Oberkampf did not provide any vapor-screen visualizations, he did provide detailed data from which velocity profile through the separated region can be plotted. The first series, Figure 24, are the vertical velocity profiles along the lee plane of symmetry for several z-stations. The size of the separated region (i.e. y_{stag} = y where $v/V_\infty = 0$) is predicted fairly well, but the peak of the maximum vertical velocity component is underpredicted. It is not a radial mesh resolution problem since an increase of the number of radial points (between the body and bow shock wave) from 30 to 40 did not improve the results. However, it could be that not enough circumferential points are in the separated region. This seems to be borne out by the following three sets of figures. These figures show the vertical velocity profiles along horizontal lines. Figure 25 is for the horizontal line at $y/D = 0.3$. Figures 26 and 27 are for $y/D = 0.6$ and 0.9, respectively. In all these curves the profiles seem to be excessively smeared. This is indicative of not enough mesh resolution, which has the tendency to reduce the sharp velocity gradients in the recirculating region.

5.3.2 Five Caliber Tangent-Ogive Cylinder.- The second case considered in this section is a 5 caliber tangent-ogive nose and cylinder combination at $M_\infty = 2.9$ and $\alpha = 20°$. For this case the numerical computations of Pulliam (ref. 18) based on the parabolized Navier-Stokes (PNS) equation are available. The PNS code is based on the steady Navier-Stokes equations. For a supersonic axial velocity the equations are hyperbolic in that

direction and a marching procedure is employed. In the boundary-layer region where the velocity becomes subsonic special techniques are employed to maintain the hyperbolic form of the Navier-Stokes equations over the entire flow field. The thin layer model is also employed, which means that only the viscous diffusion in the direction normal to the body surface is retained. Diffusion terms in the streamwise and crossflow direction are neglected.

The first set of results (Figs. 28(a) and 28(b)) shows the crossflow velocity vectors from the Euler/Kutta code and the PNS code computations. As expected there are large differences near the surface due to the viscous effects. What is not expected however are the large differences between the size and center location of the separated region. The Euler/Kutta code predicts a vortex center at about $y/D \approx 1.2$ and the PNS code at about $y/D \approx 0.7$. Similarly the heights of the recirculating region are $y_{stag} \approx 2.0D$ and $1.1D$ for the Euler/Kutta and PNS codes, respectively. These results seem to cast some serious doubts on the Euler/Kutta procedure. However, comparing the two numerical results with extensive experimental data (ref. 12) reveals that the Euler/Kutta results falls within the expected range of values determined experimentally, Figure 29, for the height of the recirculation region at $z/D = 10$. The PNS code result, on the other hand, completely underpredicts the height of the recirculating region.

The main cause for this discrepancy is probably the lack of resolution for the PNS code results in the region of the separated flow outside the boundary layer. Although the resolution is not that much better for the Euler/Kutta results, lack of resolution is much more important for the PNS code. This code is based on an implicit scheme which has a much higher dissipation inherent in the algorithm than the explicit MacCormack's scheme used for the Euler/Kutta code. Thus the implicit scheme dissipation is much

more mesh size dependent than the MacCormack scheme. This may be possibly another advantage in the Euler/Kutta procedure. Namely, reasonably good results are obtained with a fairly coarse mesh.

A comparison of the execution time for the two codes can be made. The Euler/Kutta code requires about 1000 seconds on the CDC 7600 computer to advance the solution to a station 16 calibers downstream of the nose tip for a mesh of 30 radial and 36 circumferential points. The PNS code requires about 1100 seconds to advance the solution to the same streamwise stations for a mesh of 40 radial and 24 circumferential points. It is clear, however, that the circumferential resolution for the PNS code is inadequate. If the comparison is made on the basis of the same circumferential resolution, then the PNS code requires about 1600-1700 seconds. This assumes that the radial resolution of 40 points is adequate. Thus the PNS code requires about 60 to 70 percent more computer time than the Euler/Kutta procedure, even though the implicit algorithm is more efficient. That is, it has no stability limitations on the marching step size.

6. CONCLUSIONS AND RECOMMENDATIONS

This report addressed the problem of computing the steady inviscid rotational supersonic flows about tangent ogive cylinders. At high angles of attack the flow separates into a pair of counter-rotating vortices on the lee side of the cylinder. These vortices have an adverse effect on the lift of any wings or fins attached to the cylinder. Previous studies of the body vortices include the vortex-cloud method of Mendenhall (ref. 12) and numerical calculations using the parabolized Navier-Stokes equation by Pulliam (ref. 18). The vortex-cloud method is based on Stratford's separation criterion which is not applicable if the crossflow Mach number is greater than 0.6. The numerical

calculations of Pulliam are rather lengthy even though they are based on the parabolized version of the more complete Navier-Stokes equations.

We have calculated separated flows with symmetric vortices on tangent ogive cylinders. The inviscid steady Euler equations have been used as the basic governing equations as opposed to the more complicated Navier-Stokes equations to obtain a more efficient procedure. The viscous effects, important only near the separation lines, are simulated by a Kutta condition. The rest of the flow field is essentially controlled by the inviscid equations.

The steady Euler equations were written in conservation form in generalized curvilinear coordinates. The general coordinate system was fitted to a cylindrical body by a conformal transformation between the body and a unit circle. The outer radial mesh points were adjusted to the bow shock wave by normalizing the radial coordinate between the body and the shock. Although only circular bodies were considered in this report, the conformal transformations will facilitate the application of this procedure to noncircular bodies and wing-body combinations later. The equations were approximated by MacCormack's second-order accurate predictor-corrector algorithm (ref. 14) with special stabilizing terms appended. The flow tangency conditions at the body surface were satisfied by Abbett's scheme (ref. 15) and the outer bow shock position by the Rankine-Hugoniot jump relations. Any internal shock waves or tangential discontinuities were captured by the scheme.

The Euler equations and Kutta condition approach was used in a previous study of planar delta wings and wing-body combinations (ref. 3). For these configurations with sharp leading edges the separation line was known a priori. For the tangent ogive cylinder considered in this report, the separation line could not be determined from inviscid theory. For this reason,

empirical data were required to determine the separation lines. A parametric study of the various parameters that affect the flow separation lines off the body indicated that the overall flow field is relatively insensitive to the fine details near the separation point. The most important parameter was the location of the separation line on the body. The orientation of the tangential discontinuity sheet relative to the body is of only secondary importance in controlling the overall flow field. The question of determining the pressure and density at the body separation points is still open. But, nevertheless, good results were obtained with simple linear interpolation and with a fairly coarse mesh. A finer mesh produced better overall results and a smoother pressure distribution on the body. It turned out that specifying a variable separation line on the nose region did not greatly influence the results further downstream as long as the proper asymptotic value of the separation angle was finally reached. Specifying the asymptotic value along the entire length produced similar results. The variable separation line produced only minor coding problems. A second Kutta condition could be applied to obtain the secondary separated flow. However, it is not known how important this secondary separation may be. It is suspected that it will give better surface pressure results in the separated flow region and have very little influence elsewhere.

It was also shown that the Euler/Kutta codes gave results which agreed well with experimental data. These results were obtained for much lower run times than those from the PNS code. It is anticipated that these costs could be further reduced (by a factor of two or three) if the explicit algorithm used in the code is replaced by the more efficient implicit codes used for the PNS code.

We have shown that the Euler/Kutta procedure works well for smooth bodies such as cylindrical bodies with tangent-ogive

noses considered in this report as long as empirical data are available to specify a priori the separation line. The application of this procedure for sharp-edge bodies such as wings has been demonstrated in the previous year's work. Therefore we are now in a position to compute the interaction problem of a complete missile configuration. This problem can include the interaction of the forebody vortices with the wings and the wing vortices as well as wing-tail interference.

However, before such a capability to solve a complete missile configuration is established, it is recommended that the following work be carried out.

1. The determination of the pressure and density at the separation line on the body needs further clarification.
2. The implicit algorithm should be adapted for the Euler/Kutta code. This will further reduce the computation time by a factor of two or three.
3. The effects of including secondary separation points on the forebody vortices should be assessed.
4. Finally, a separation criterion for supercritical cross-flow should be established from empirical data. Incorporation of this separation criterion will make the Euler/Kutta code independent of any specific set of empirical data and thus much more useful.

REFERENCES

1. Nielsen, J. N.: Nonlinearities in Missile Aerodynamics. AIAA Paper No. 78-20, Invited paper, AIAA 16th Aerospace Sciences Meeting, Huntsville, AL, Jan. 16-18, 1978 (also NEAR Paper No. 63).

2. Nielsen, J. N., Hemsch, M. J., and Smith, C. A.: A Preliminary Method for Calculating the Aerodynamic Characteristics of Cruciform Missiles to High Angles of Attack Including Effects of Roll Angle and Control Deflections. Report ONR-CR215-226-4F, Nov. 1977.

3. Klopfer, G. H. and Nielsen, J. N.: Euler Solutions for Wing and Wing-Body Combination at Supersonic Speeds with Leading Edge Separation. AIAA Paper No. 80-0126, AIAA 18th Aerospace Sciences Meeting, Pasadena, CA, Jan. 14-16, 1980 (also NEAR Report TR 206).

4. Oberkampf, W. L. and Bartel, T. J.: Compressibility Effects on the Symmetric Body Vortex Wake of an Ogive Nose Cylinder. Paper presented at AGARD (NATO) Symposium on High Angle of Attack Aerodynamics, Sandefjord, Norway, 4-6 October 1978.

5. Oberkampf, W. L., Bartel, T. J., and Martindale, W. R.: Supersonic Flow Measurements in the Body Vortex Wake of an Ogive Nose Cylinder. AIAA Paper No. 78-787, April 1978.

6. Oberkampf, W.: Supersonic Flow Measurements in the Body Vortex Wakes of an Ogive Nose Cylinder. AFATL-TR-78-127, Austin, Texas, Nov. 1978.

7. Landrum, E. J.: Wind-Tunnel Pressure Data at Mach Numbers from 1.6 to 4.63 for a Series of Bodies of Revolution at Angles of Attack from -4° to 60°. NASA TM X-3558, October 1977.

8. Schiff, L. B. and Steger, J. L.: Numerical Simulation of Steady Supersonic Viscous Flow. AIAA Paper No. 79-0130, AIAA 17th Aerospace Sciences Meeting, New Orleans, LA, Jan. 15-17, 1979.

9. Chapman, G. T., Keener, E. R., and Malcolm, G. N.: Asymmetric Aerodynamic Forces on Aircraft Forebodies at High Angles of Attack - Some Design Guides. Paper published in AGARD Conference Proceedings No. 199 on Stall-Spin Problems of Military Aircraft, Nov. 1976.

REFERENCES (Concluded)

10. Vigneron, V. C., Rakich, J. V., and Tannehill, J. C.: Calculation of Supersonic Viscous Flow Over Delta Wings with Sharp Subsonic Leading Edges. AIAA Paper No. 78-1137, AIAA 16th Aerospace Sciences Meeting, Huntsville, AL, Jan. 16-18, 1978.

11. Spangler, S. B. and Mendenhall, M. R.: Further Studies of Aerodynamic Loads at Spin Entry. Report ONR-CR212-225-3, June 1977.

12. Mendenhall, M. R., Spangler, S. B., and Perkins, S. C., Jr.: Vortex Shedding from Circular and Noncircular Bodies at High Angles of Attack. AIAA Paper No. 79-0026, Jan. 1979.

13. Kutler, P., Warming, R. F. and Lomax, H.: Computation of Space Shuttle Flow Fields Using Noncentered Finite-Difference Schemes. AIAA Journal, Vol. 11, No. 2, Feb. 1973, pp. 196-204.

14. Kutler, P. and Lomax, H.: Shock-Capturing, Finite Difference Approach to Supersonic Flows. J. of Spacecraft & Rockets, Vol. 8, No. 12, Dec. 1972, pp. 1175-1187.

15. Abbett, M. J.: Boundary Condition Computational Procedures for Inviscid Supersonic Steady Flow Field Calculations. Aerotherm Corp., Mountain View, CA, Final Report 71-41, 1971.

16. Peake, D. J. and Tobak, M.: Three-Dimensional Interactions and Vortical Flows with Emphasis on High Speeds. NASA TM 81169, March 1980.

17. Mendenhall, M. R.: Predicted Vortex Shedding from Noncircular Bodies in Supersonic Flow. AIAA Paper No. 80-1559, AIAA Atmospheric Flight Mechanics Conference, Danvers, MA, August 11-13, 1980.

18. Pulliam, T.: Unpublished numerical results. NASA/Ames Research Center, Moffett Field, CA, May 1980.

19. Landrum, E. J. and Babb, C. D.: Wind-Tunnel Force and Flow-Visualization Data Mach Numbers from 1.6 to 4.63 for a Series of Bodies of Revolution at Angles of Attack from -4° to 60°. NASA TM 78813, March 1979.

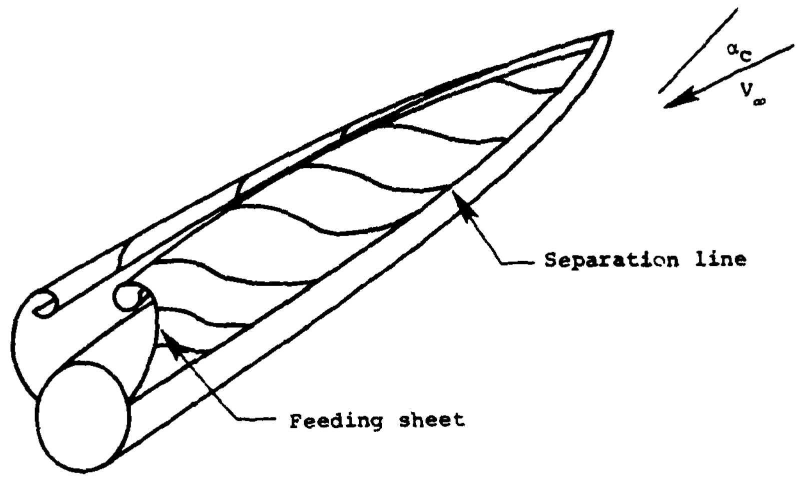

(a) Symmetric separation

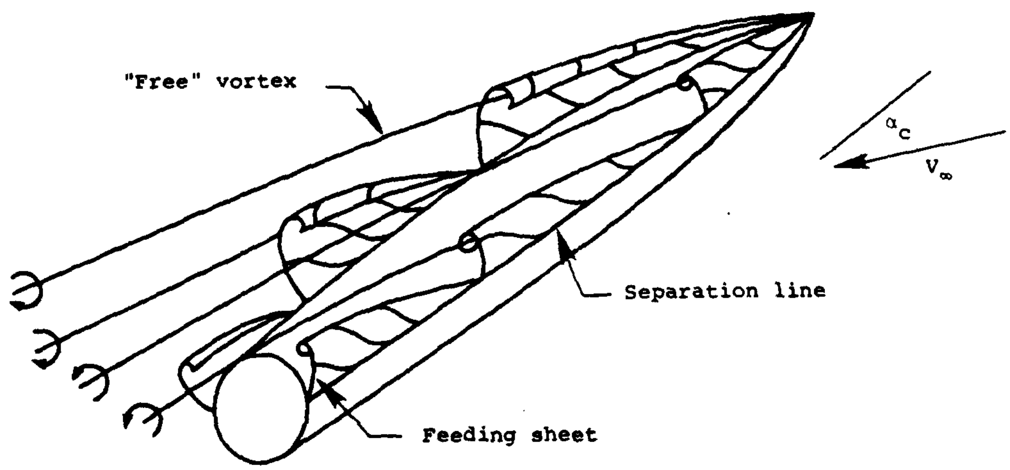

(b) Asymmetric separation

Figure 1.- Symmetric and asymmetric vortex formation.

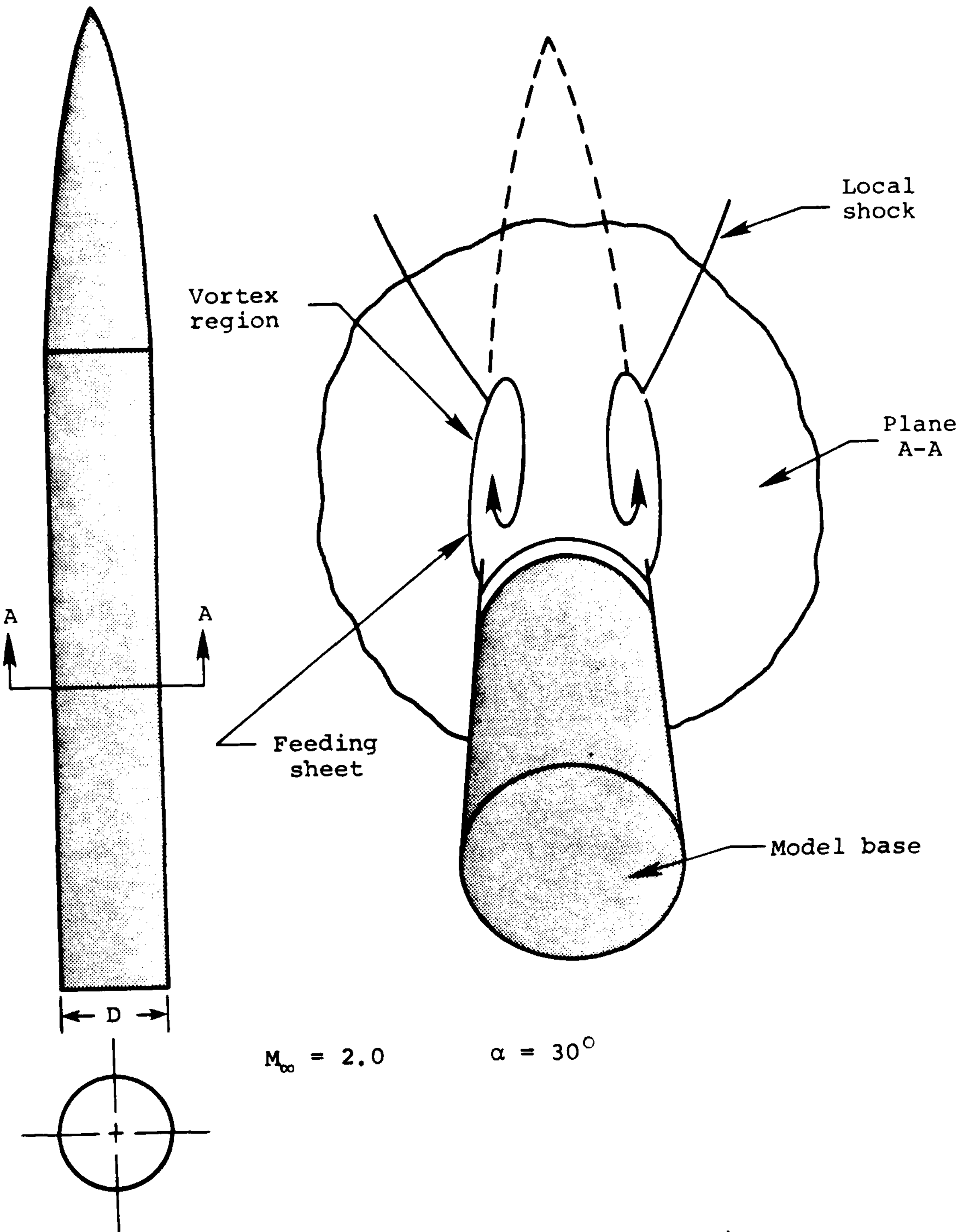

Figure 2.- Supercritical crossflow in a plane normal to axis of body of revolution.

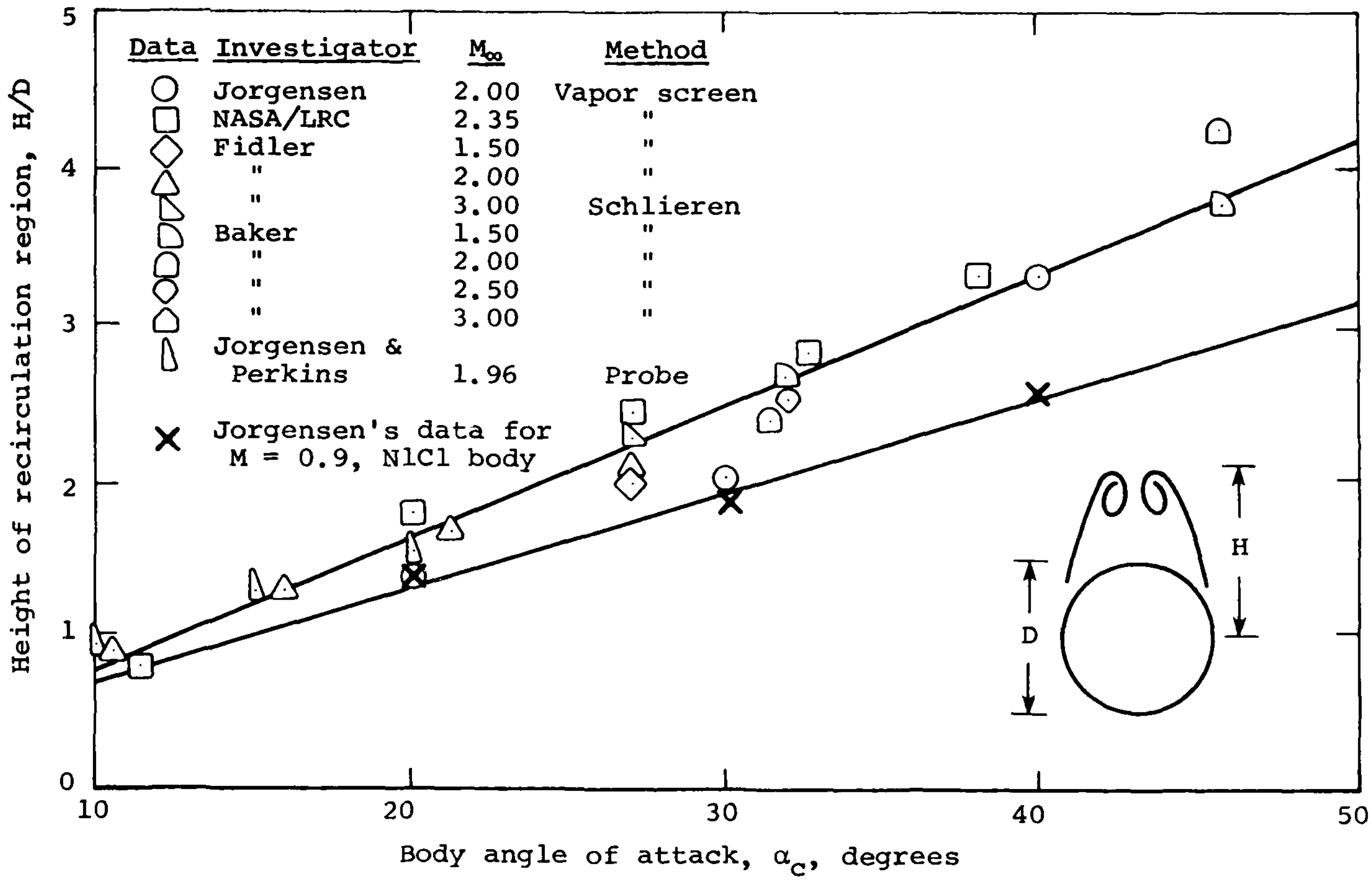

Figure 3.- Estimated height of top of recirculation region at X/D = 10 for tangent-ogive cylinder (ref. 2).

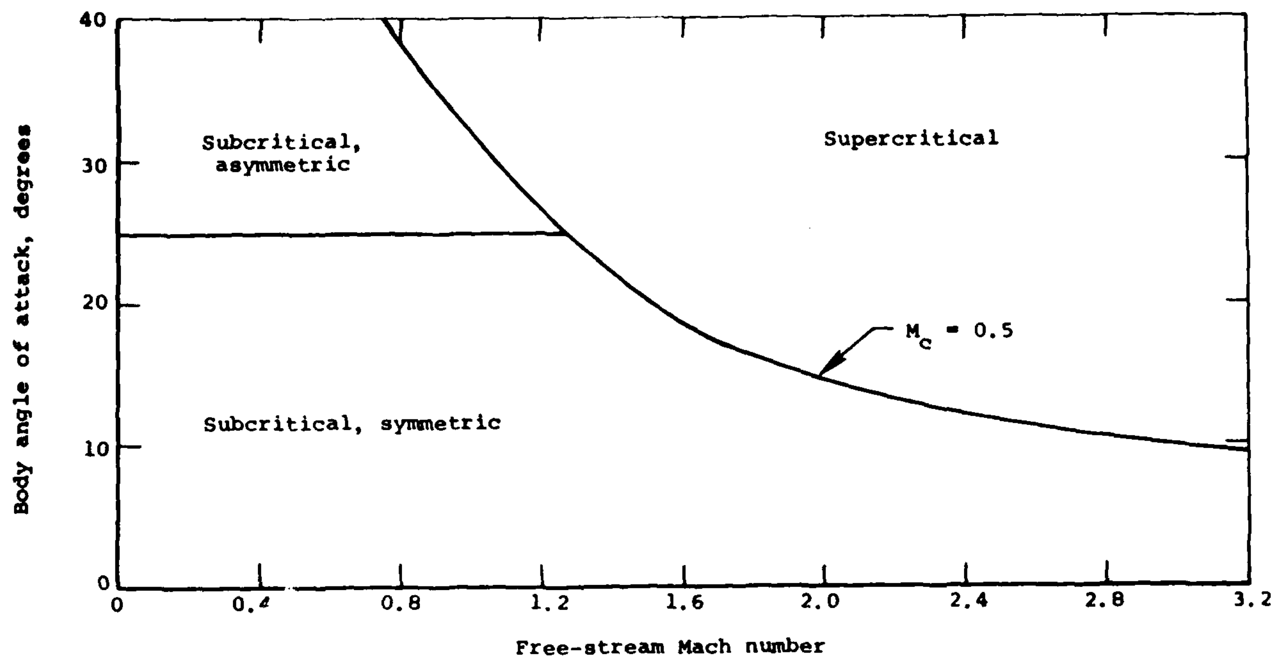

Figure 4.- Approximate regions for various types of body vortices.

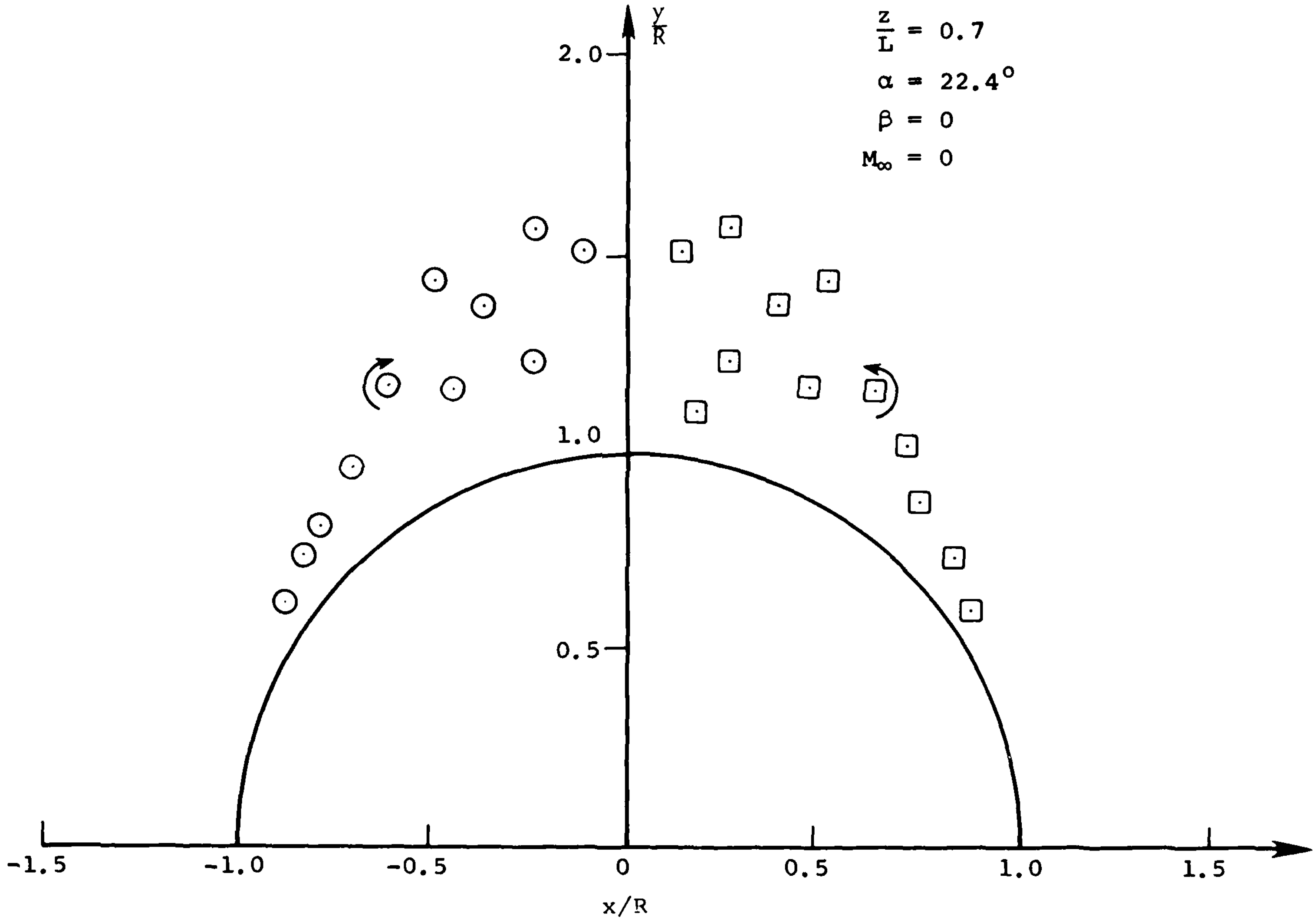

Figure 5.- Calculated symmetric vortex cloud in crossflow plane of L/D = 7 ogive-cylinder.

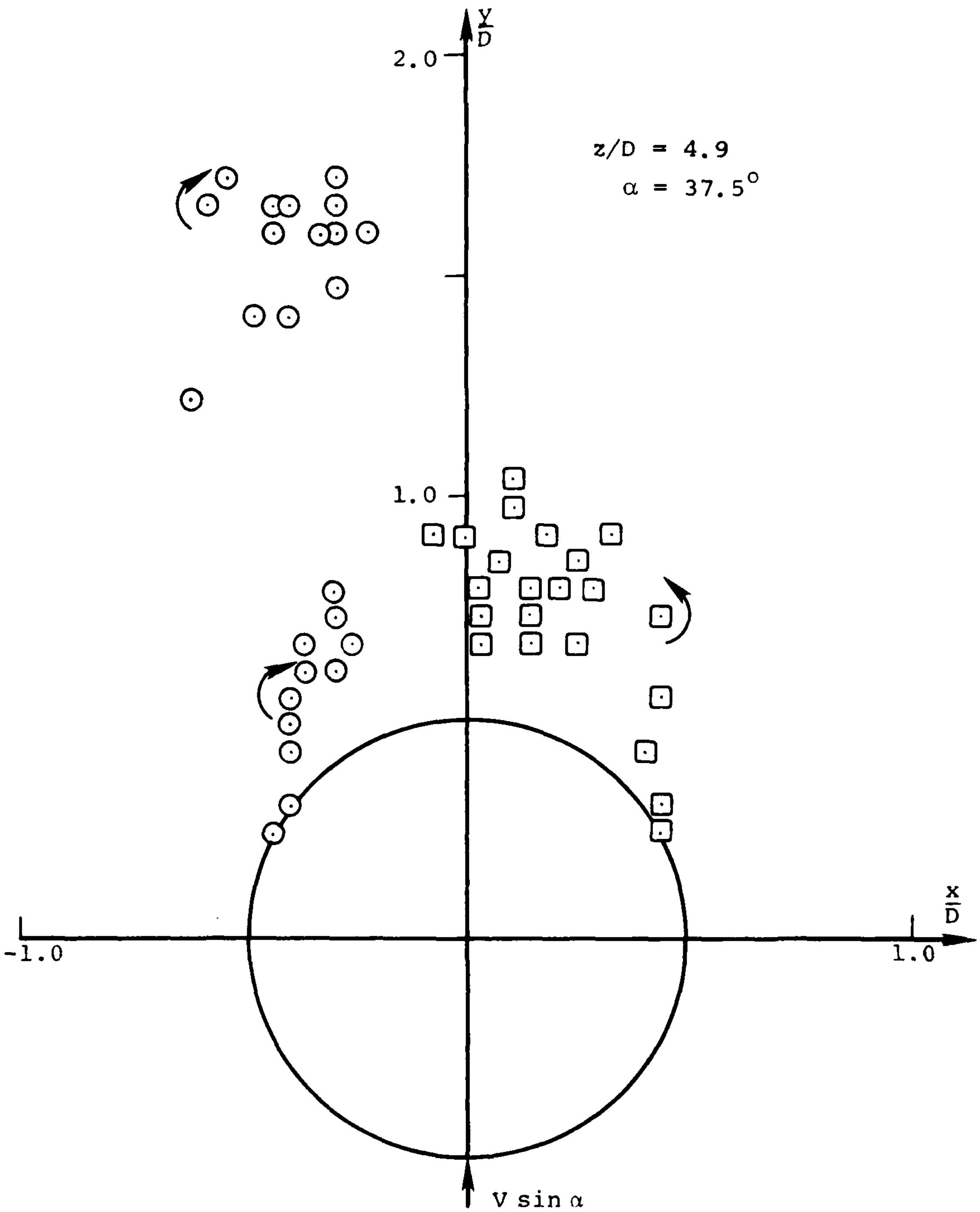

Figure 6.- Calculated asymmetric vortex cloud in crossflow plane of L/D = 7 ogive-cylinder.

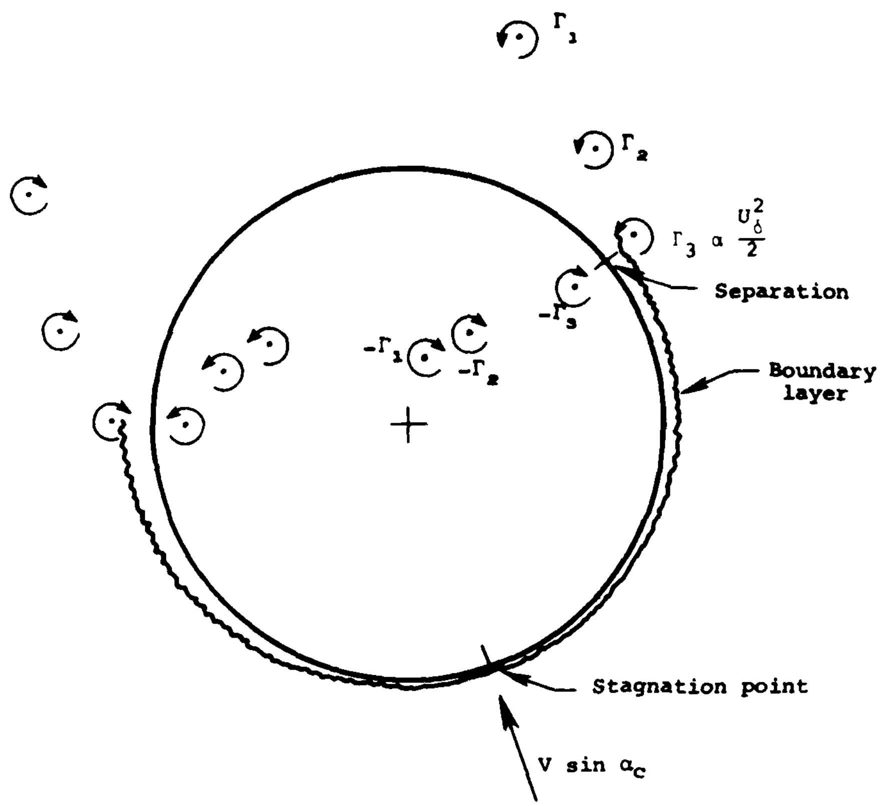

Modified Stratford Criteria

Laminar: $C_p^{1/2}\left(s \frac{dC_p}{ds}\right) = 0.102 \sin \alpha_c$

Turbulent: $C_p \left(s \frac{dC_p}{ds}\right)^{1/2} \left(Re_s \times 10^{-6}\right)^{-.1} = 0.35 \sin \alpha_c$

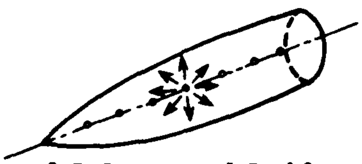

Figure 7.- Asymmetric vortex-shedding model for circular cross sections.

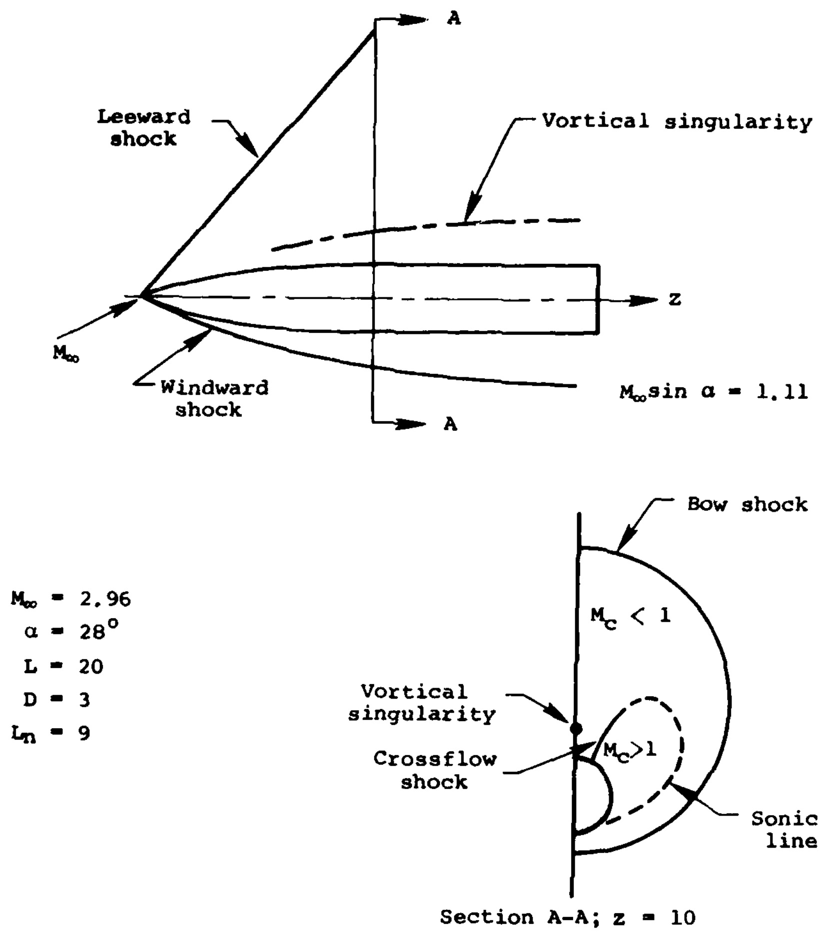

Figure 8.- Inviscid supersonic crossflow about body at high angle of attack.

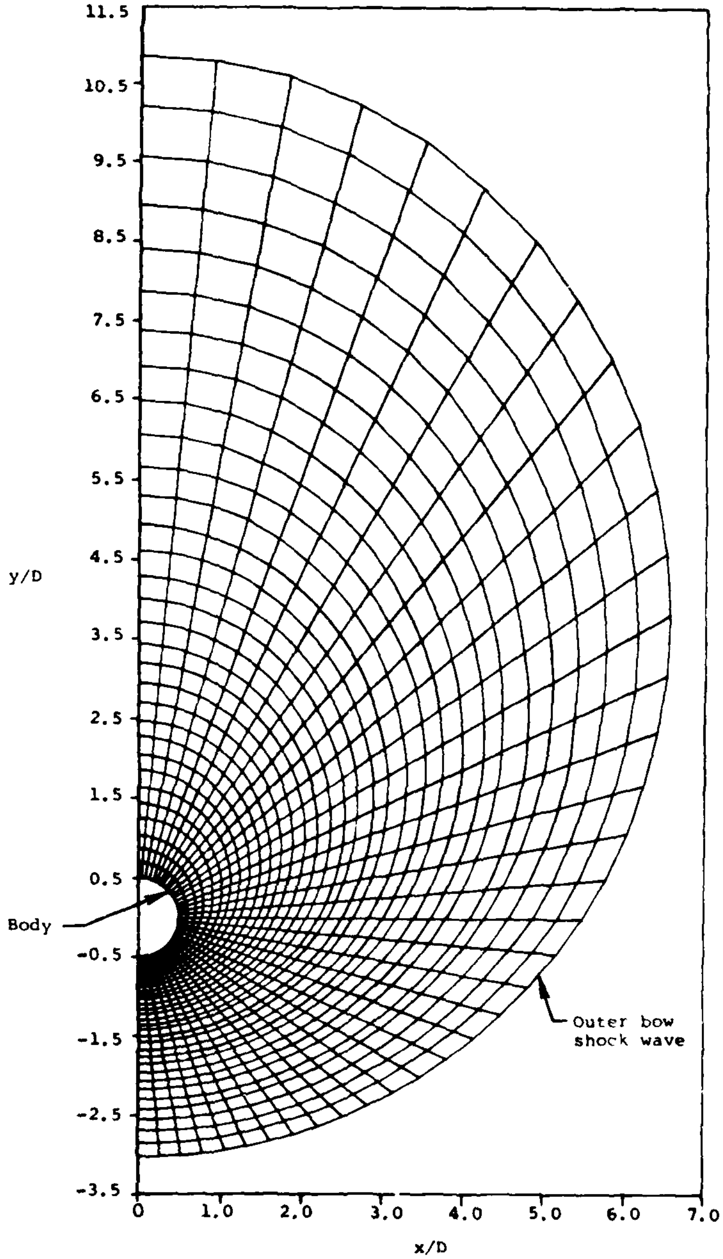

Figure 9.- Mesh for tangent ogive cylinder.

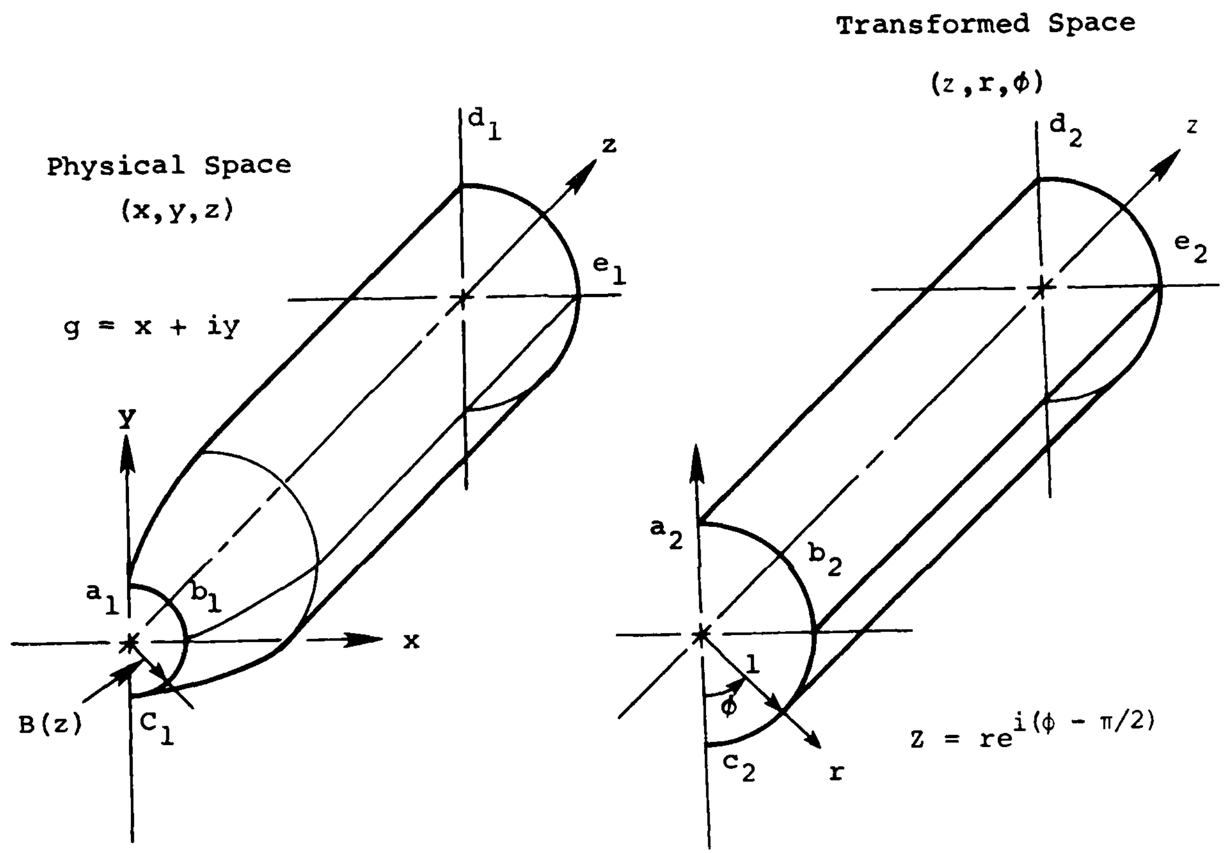

Figure 10.- The transformation between the physical space and the arbitrary curvilinear space.

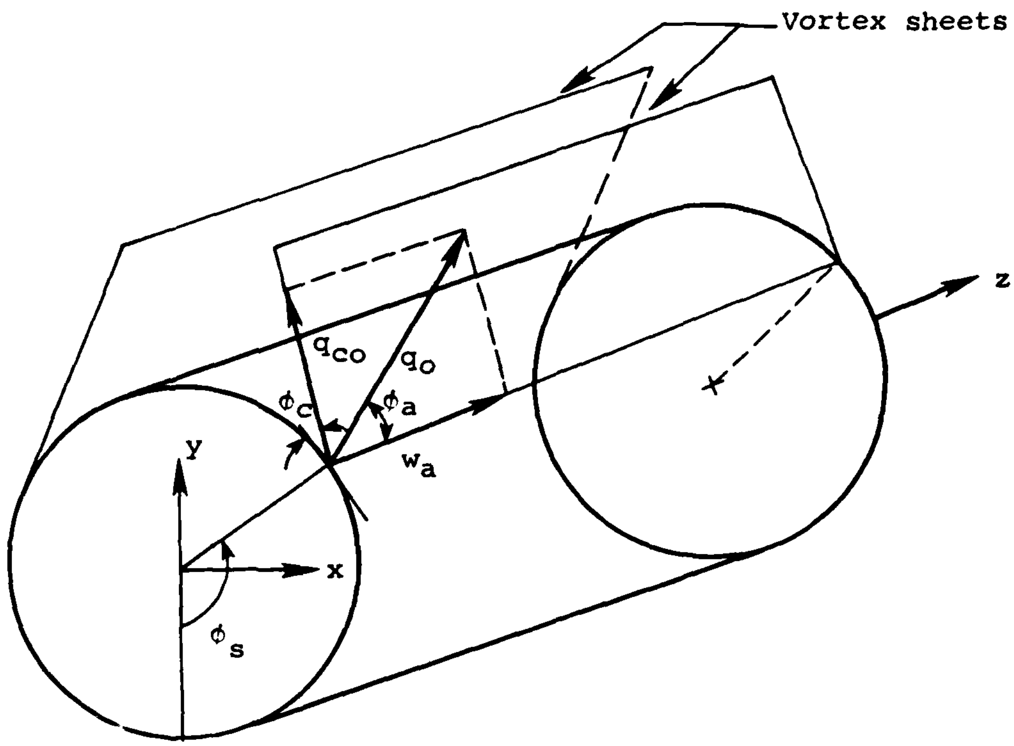

Figure 11.- Nomenclature of the velocity components and angles of the vortex sheet defining the parameters for the Kutta condition, ϕ_s: circumferential location of separation line, ϕ_c: angle between vortex sheet and tangent plane to body at separation line, ϕ_a: angle between the total velocity vector in the vortex sheet and the axial direction.

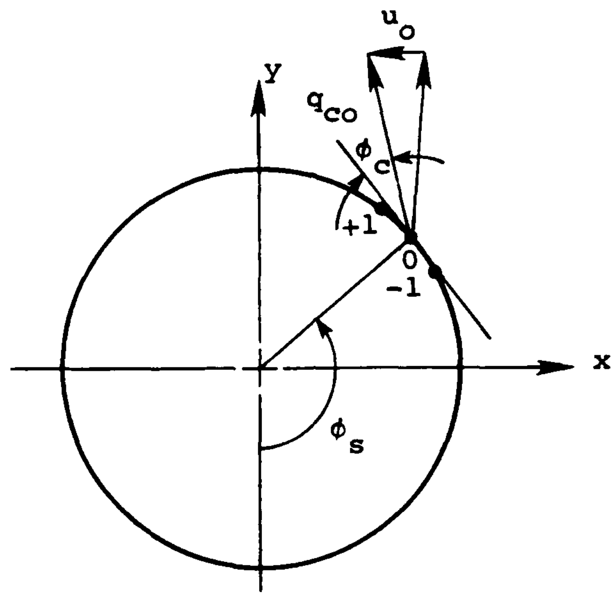

Figure 12.- Detail of separation point in the cross flow plane.

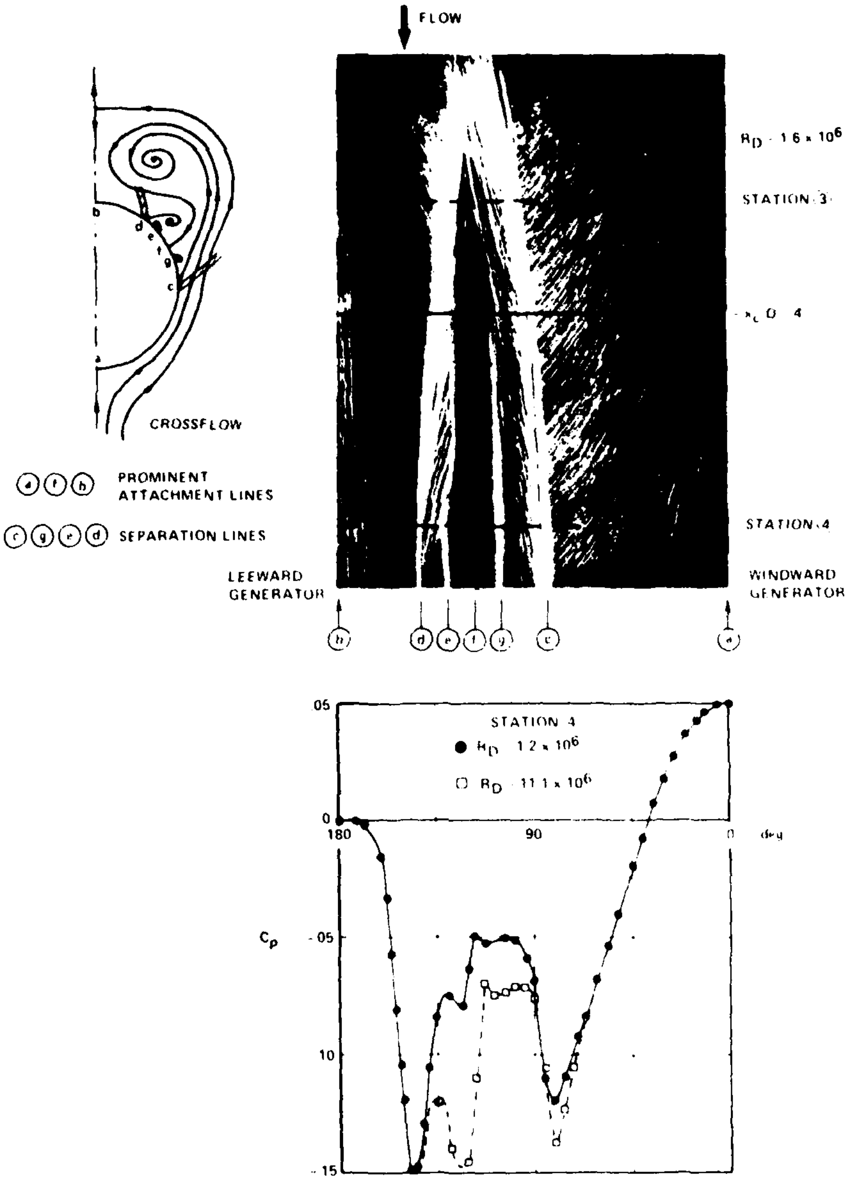

Figure 13.- Oil flow and surface pressures on downstream part of afterbody (ref. 16, fig. 95).

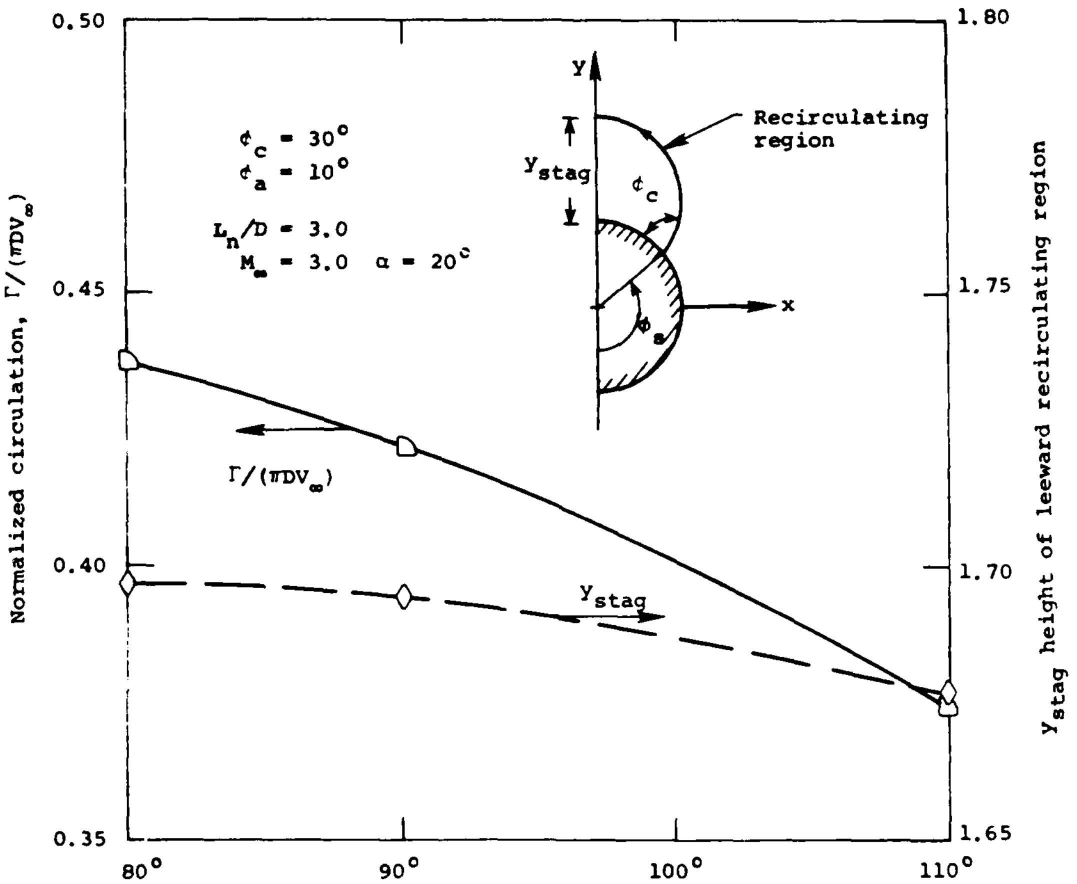

(a) Separation angle, ϕ_s

Figure 14.- Effect of the three geometric parameters on the vorticity and size of the separated flow region of a 3.0 caliber tangent ogive cylinder at z = 11 calibers.

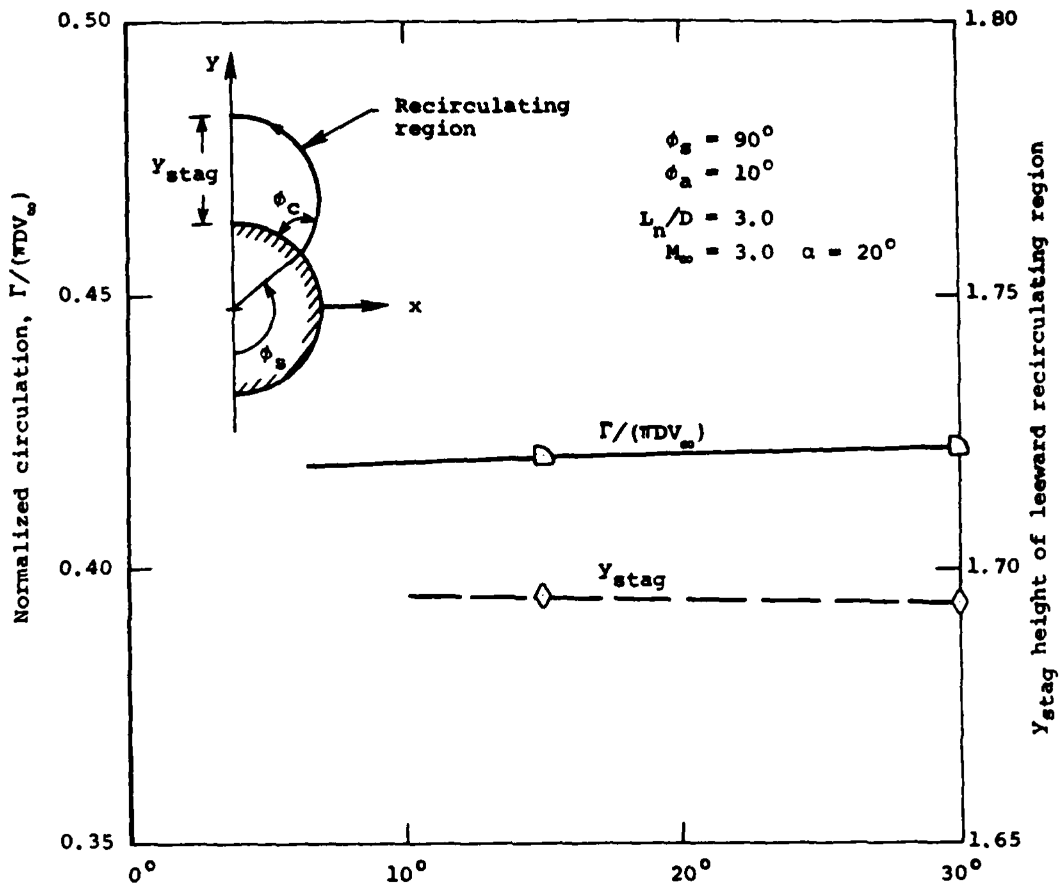

(b) Crossflow angle, ϕ_c

Figure 14.- Continued.

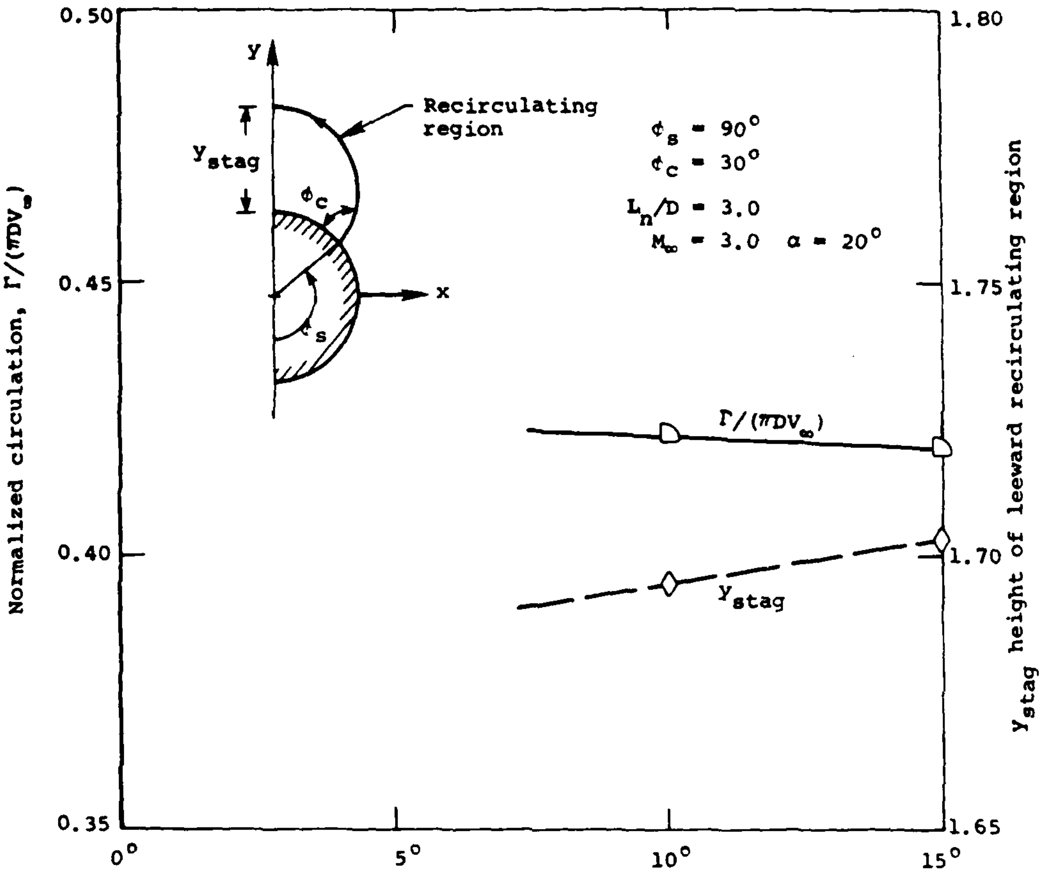

(c) Axial angle, ϕ_a

Figure 14.- Concluded.

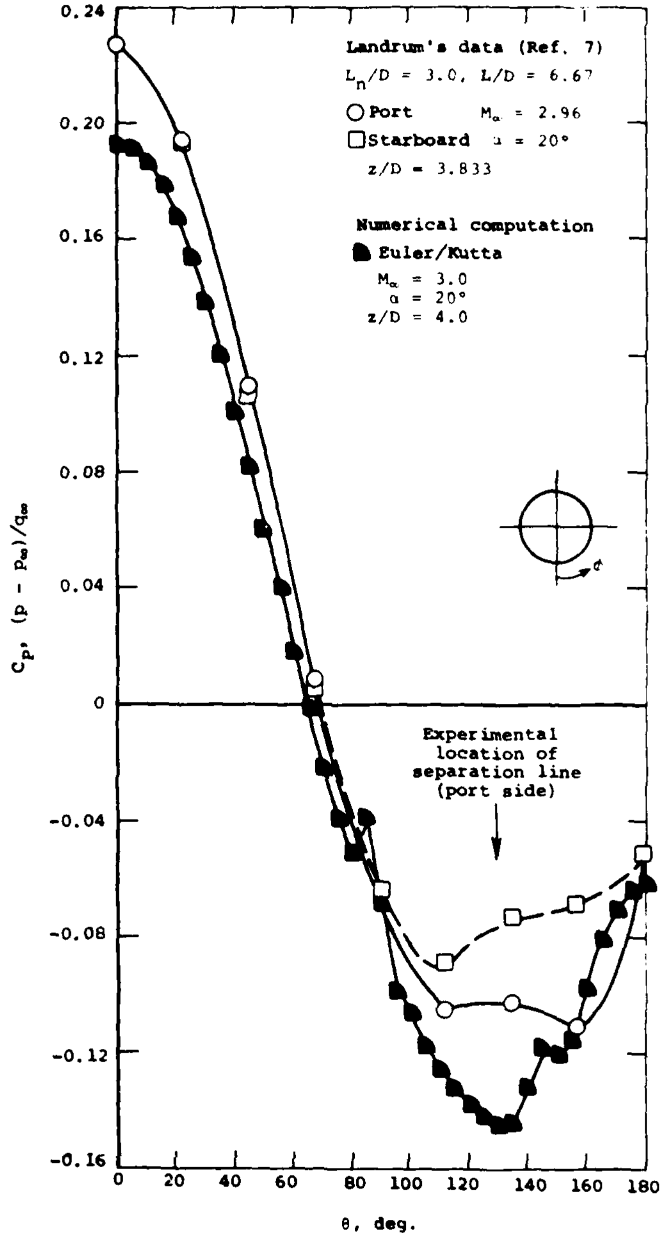

(a) z/D = 4.0

Figure 15.- Circumferential pressure distribution on a 3.0 caliber tangent-ogive cylinder at α = 20°.

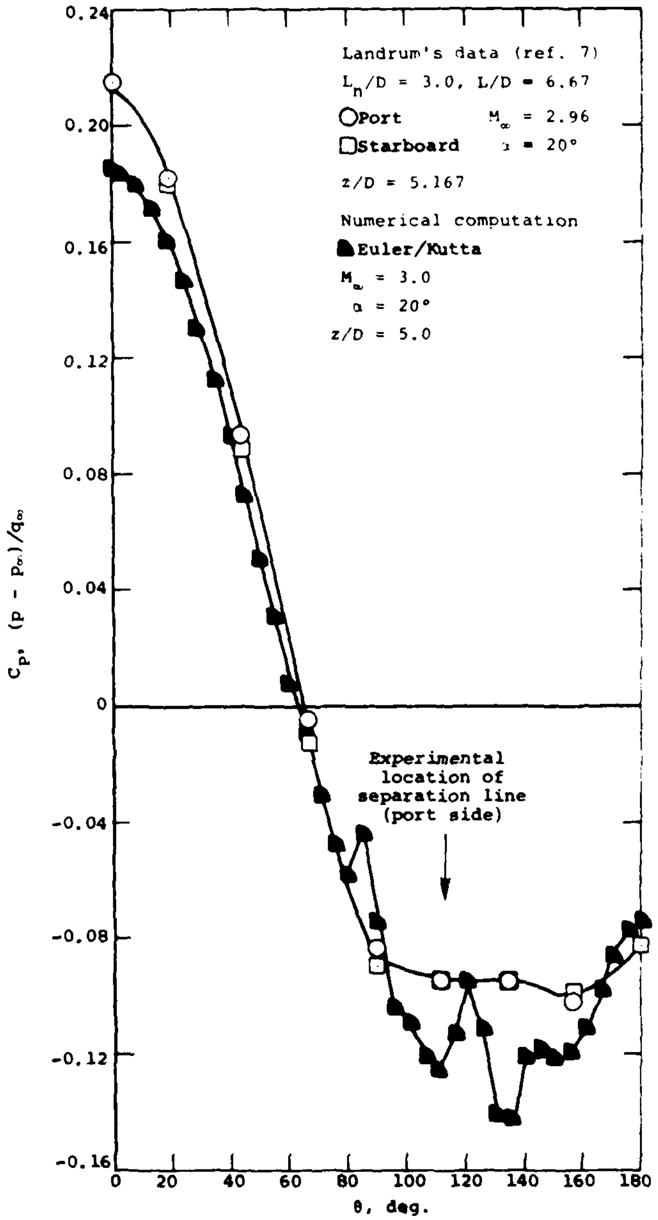

(b) z/D = 5.0

Figure 15.- Continued.

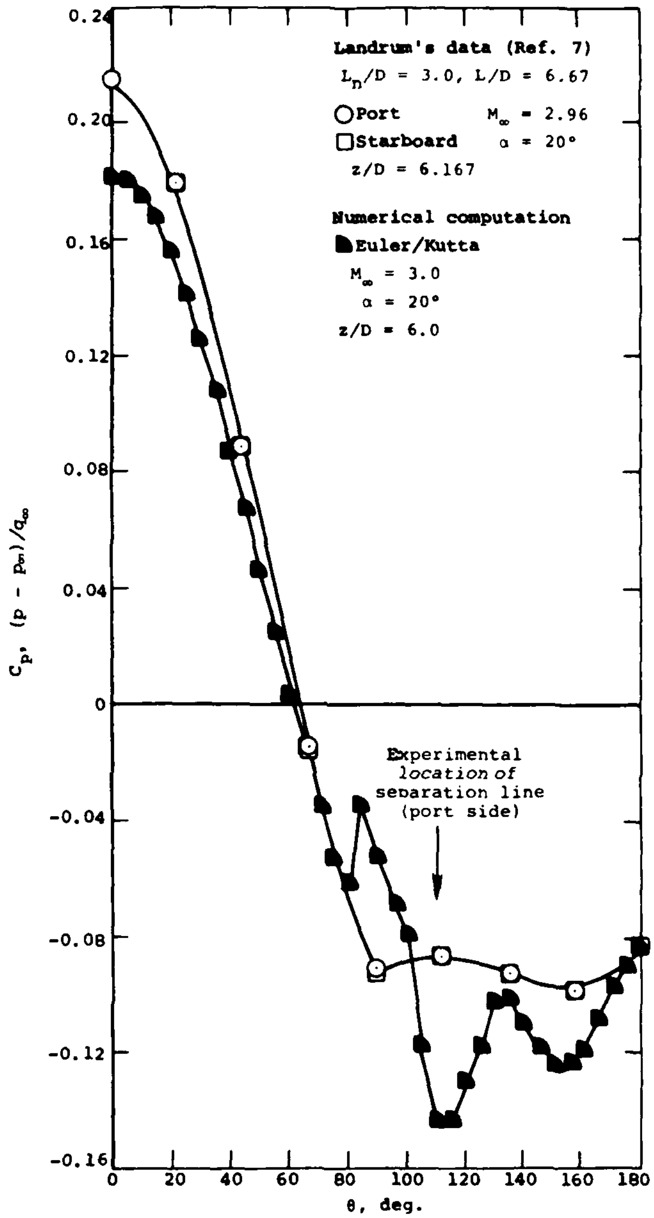

(c) z/D = 6.0

Figure 15.- Concluded.

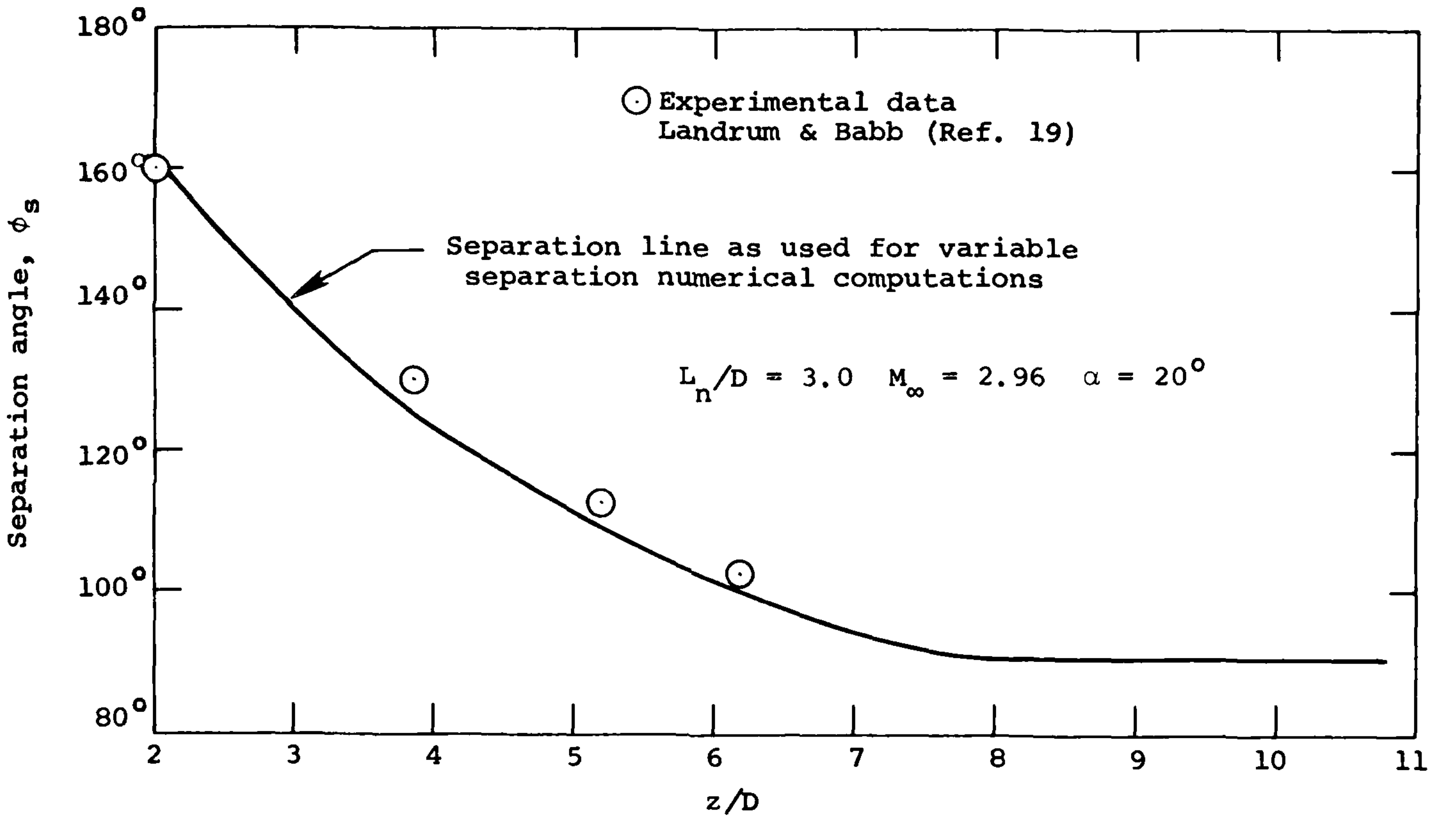

Figure 16.- Axial variation of separation line.

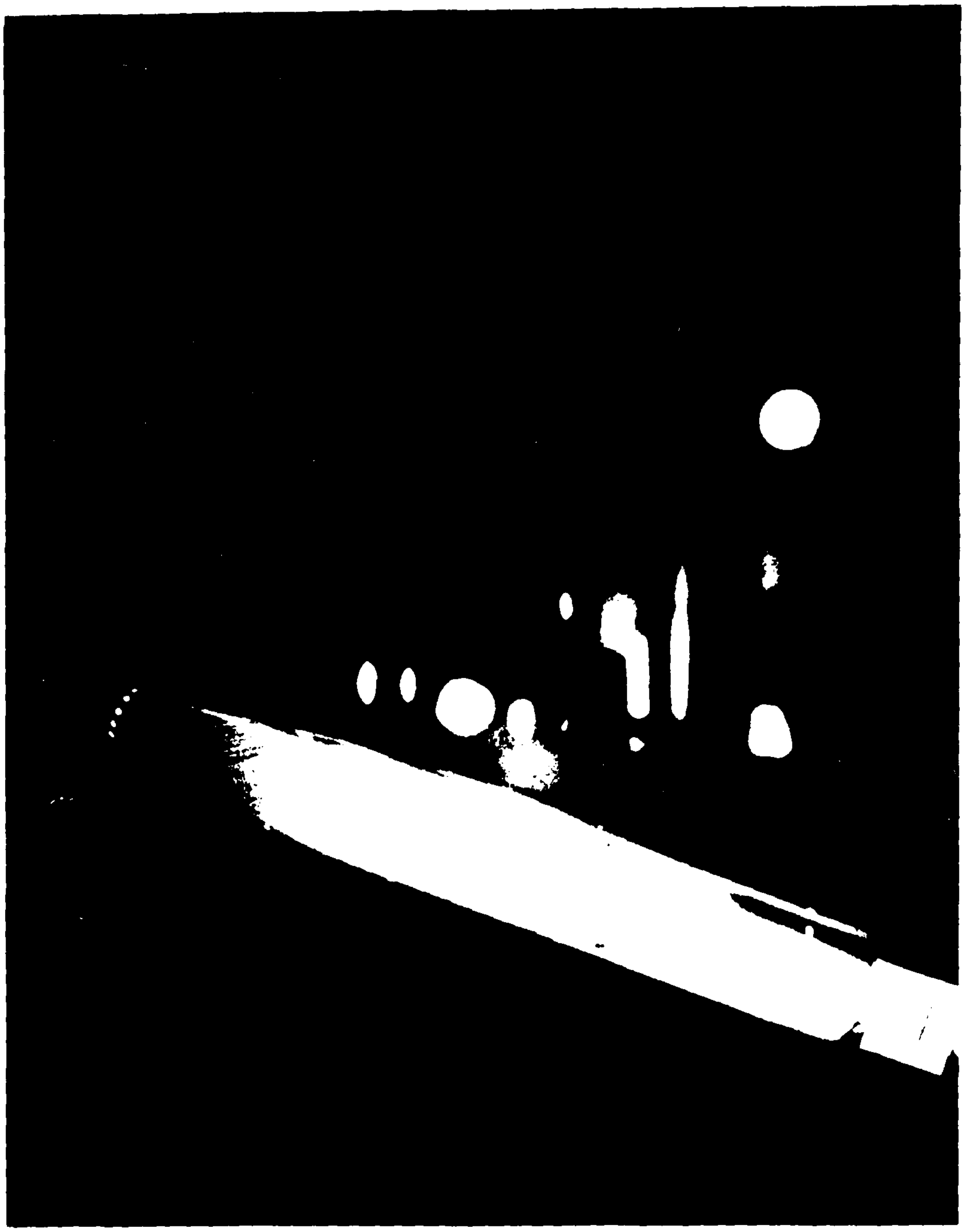

$\alpha = 20^\circ$, $M_\infty = 2.96$

Figure 17.- Oil-flow photographs for circular-arc -- cylinder model (ref. 19).

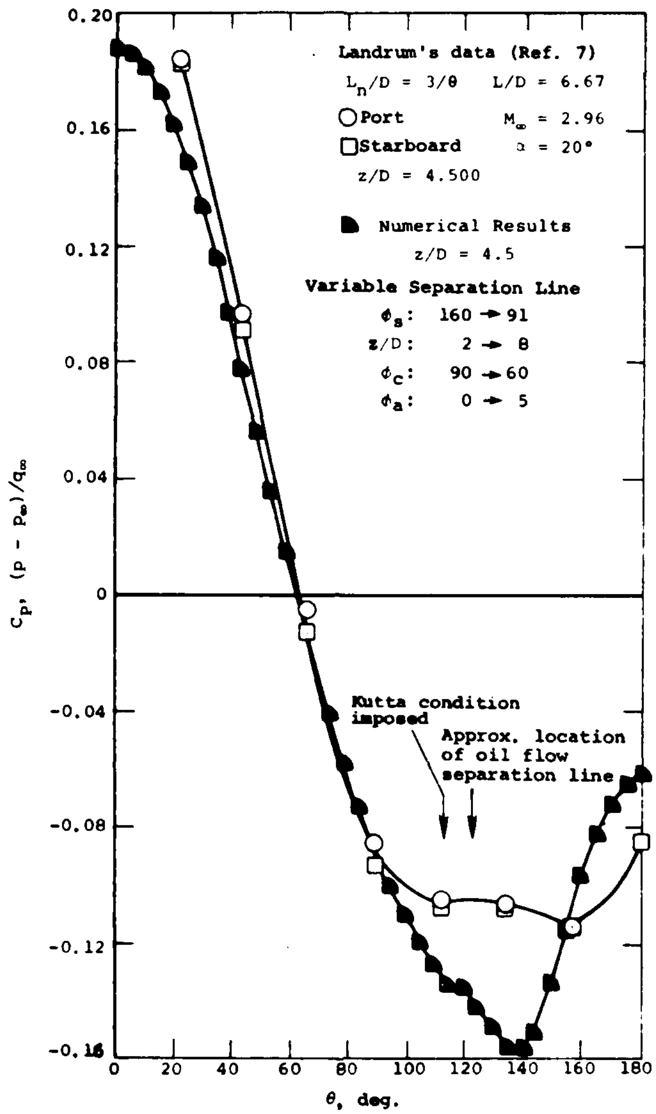

(a) z/D = 4.5

Figure 18.- Circumferential pressure distribution on a tangent-ogive cylinder at α = 20°.

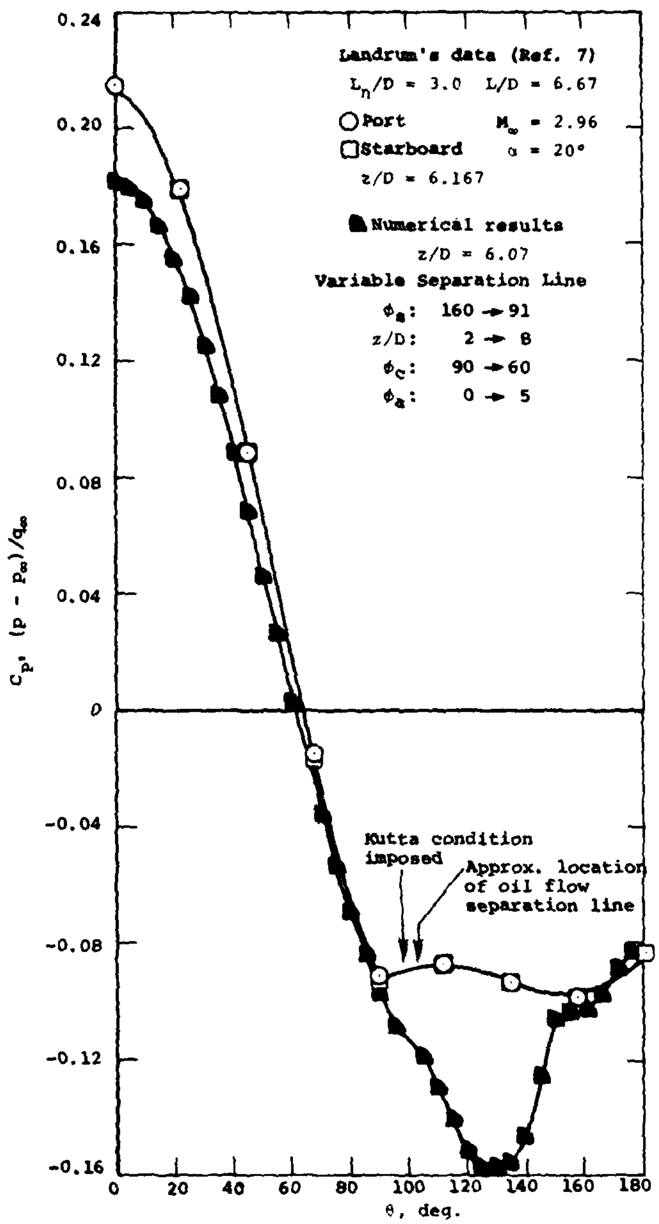

(b) z/D = 6.0

Figure 18.- Concluded.

X Numerical shock location

● Numerical upper limit of the separated region

$M_\infty = 2.96 \quad \alpha = 20^\circ$

(a) Schlieren photograph

Figure 19.- Experimental and numerical comparison for circular-arc-cylinder model (ref. 19).

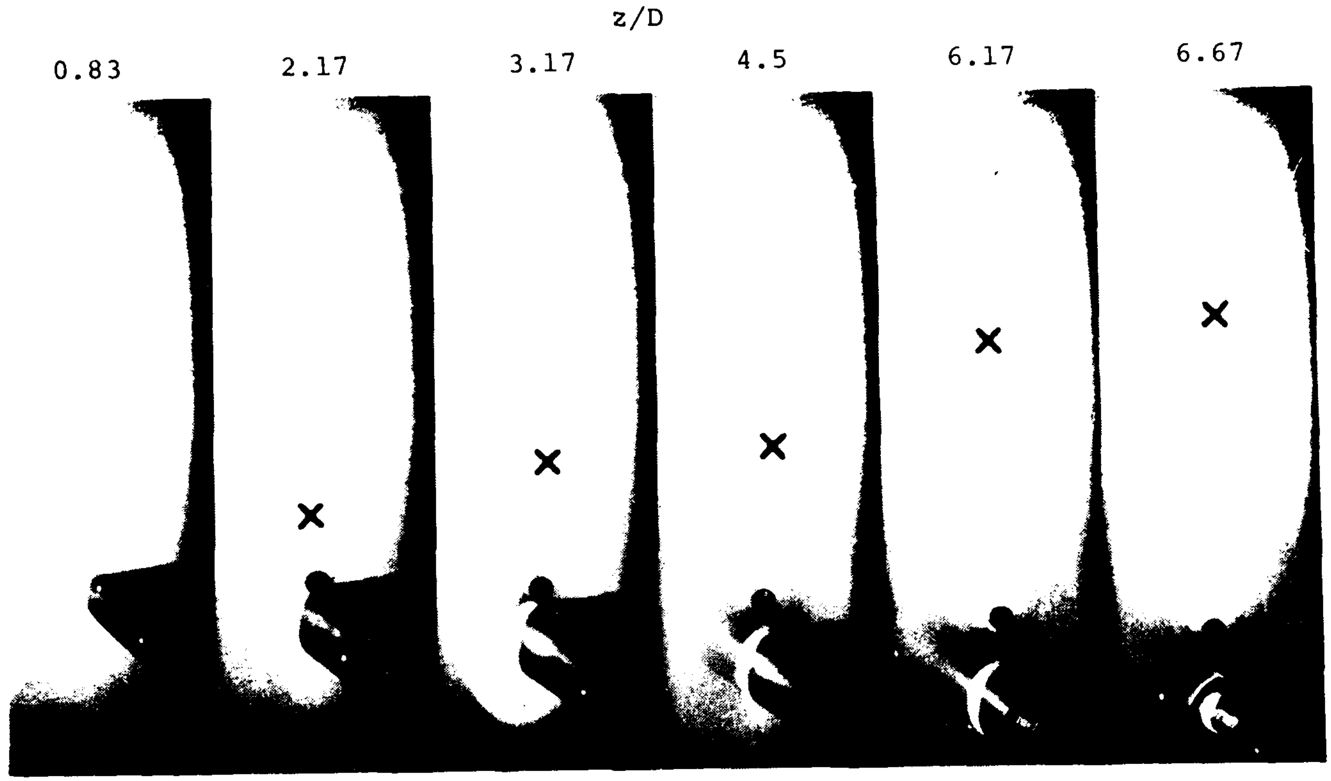

× Numerical shock location

● Numerical upper limit of the separated region

$M_\infty = 2.96 \quad \alpha = 20°$

(b) Vapor-screen photograph

Figure 19.- Concluded.

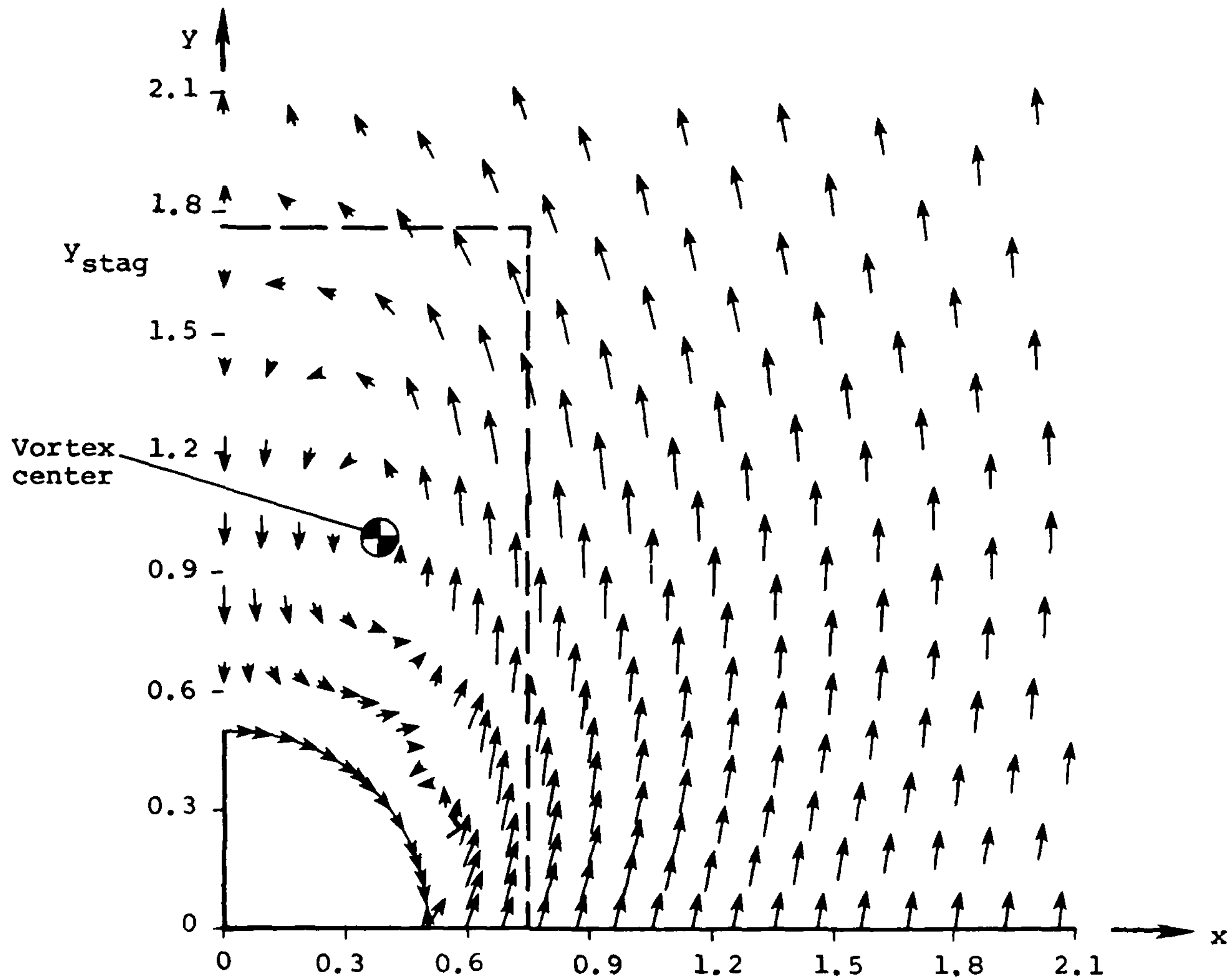

$M_\infty = 3.00 \quad \alpha = 15^\circ \quad z = 13.00$

Figure 20.- Cross flow velocity vectors Euler code with Kutta condition 2 caliber tangent-ogive nose.

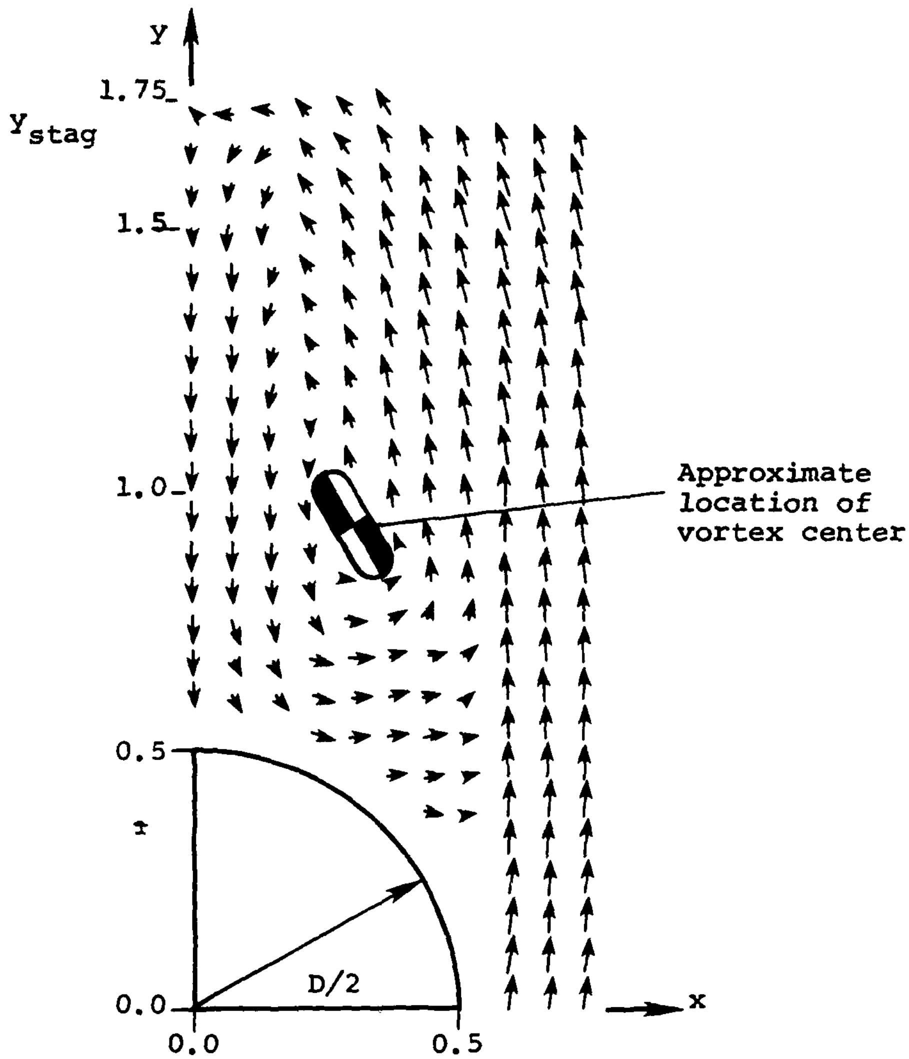

Figure 21.- Cross-flow plane vector plot for $M_\infty = 3.01$,
$R_d = 1.70 \times 10^6$ and $\alpha = 15^o$. $z/D = 13$
Oberkampf's experimental data (Ref. 6)
nose length: 2 calibers.

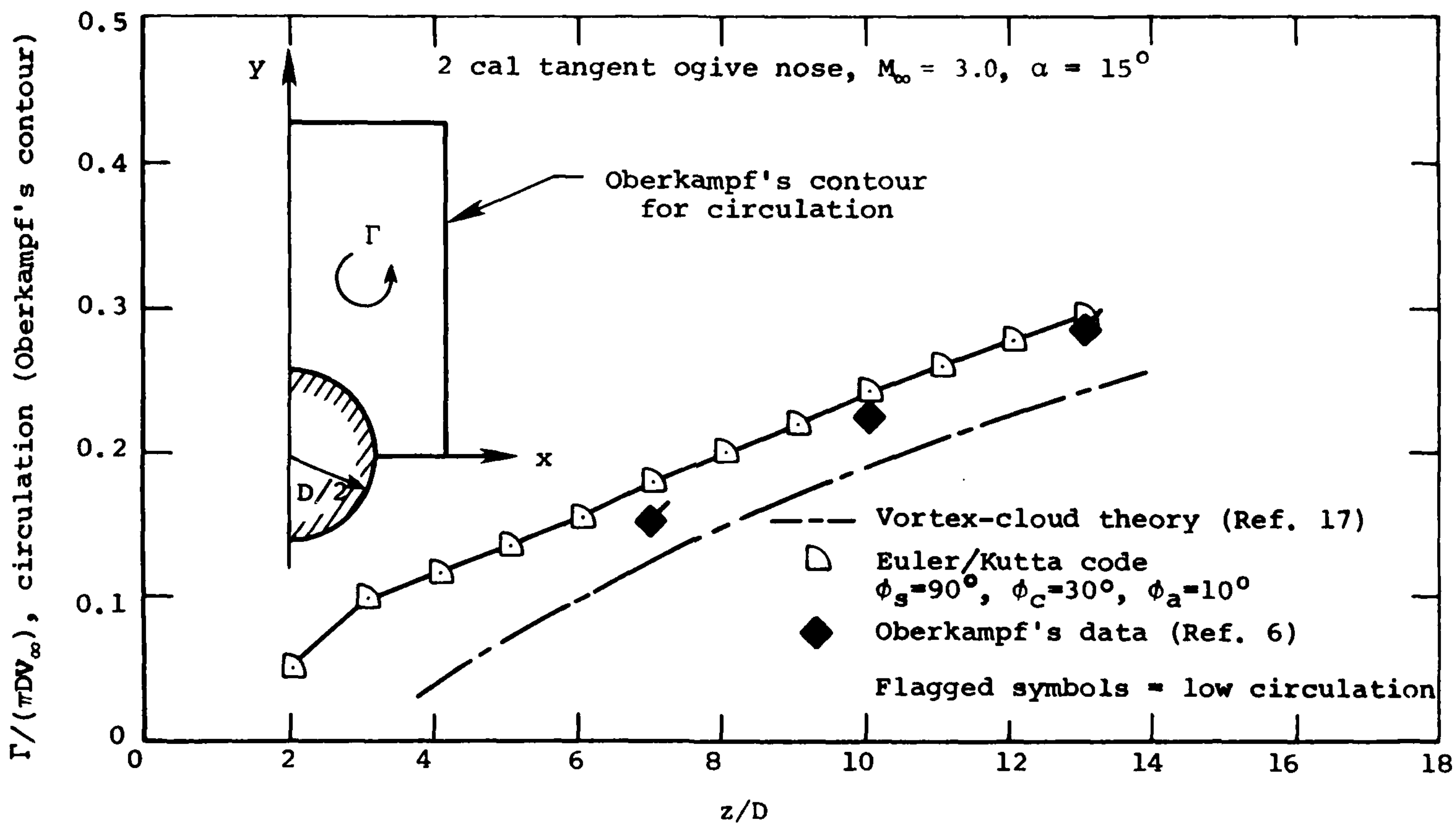

Figure 22.- Comparison of circulation for Euler/Kutta code, vortex cloud theory, and experimental data.

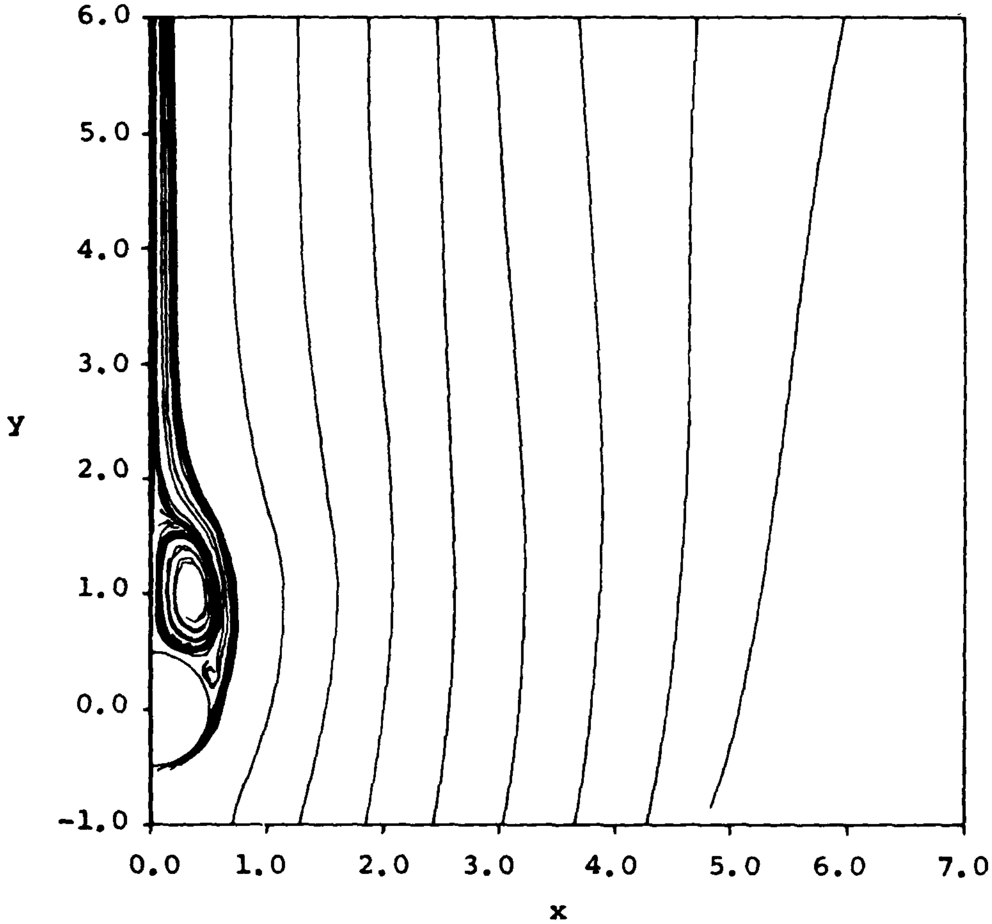

$M_\infty = 3.00 \quad \alpha = 15^o \quad Re = 0.0 \quad z = 13.00$

Figure 23.- Cross flow particles paths as determined by Euler code with Kutta condition.

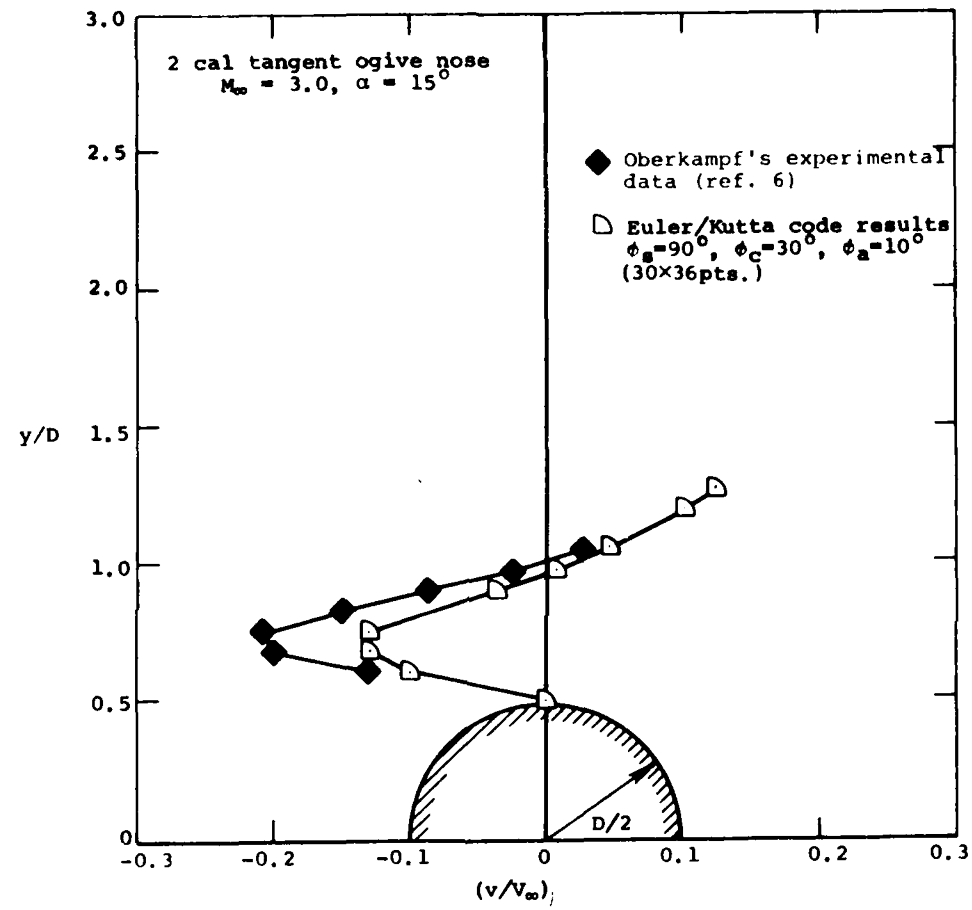

(a) z/D = 2.0

Figure 24.- Vertical velocity component on lee plane of symmetry (ϕ = 180°).

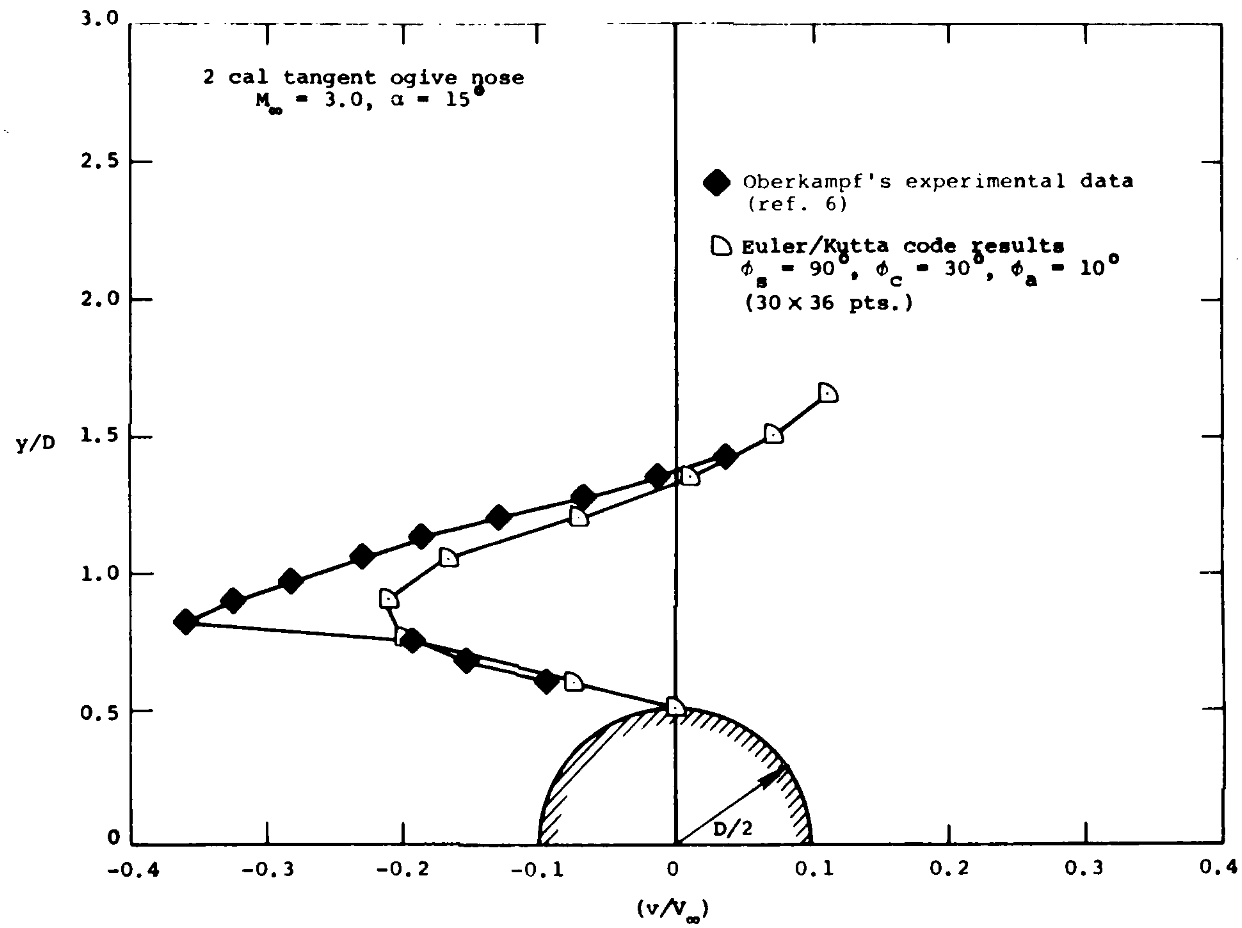

(b) z/D = 1.0

Figure 24.- Continued.

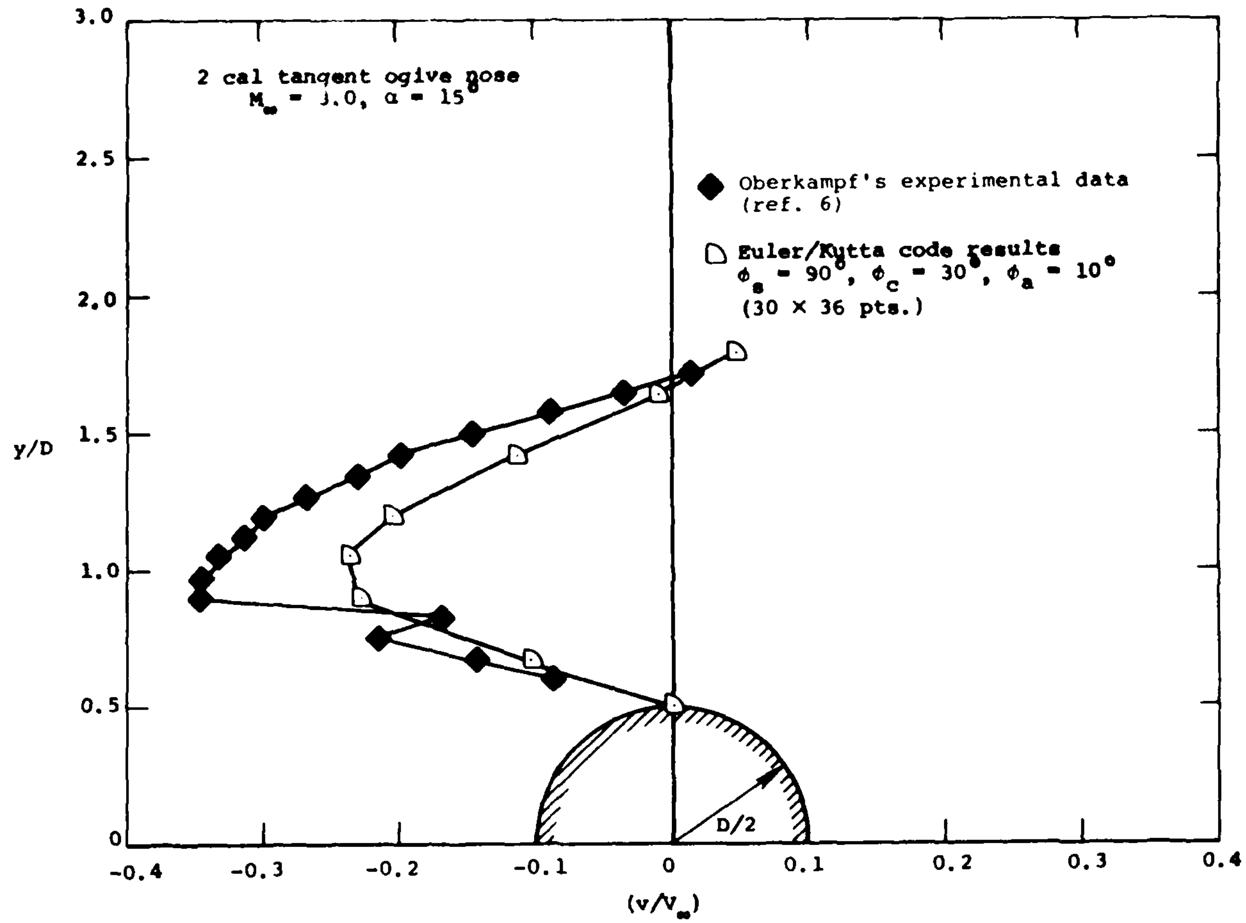

(c) z/D = 13.0

Figure 24.- Concluded.

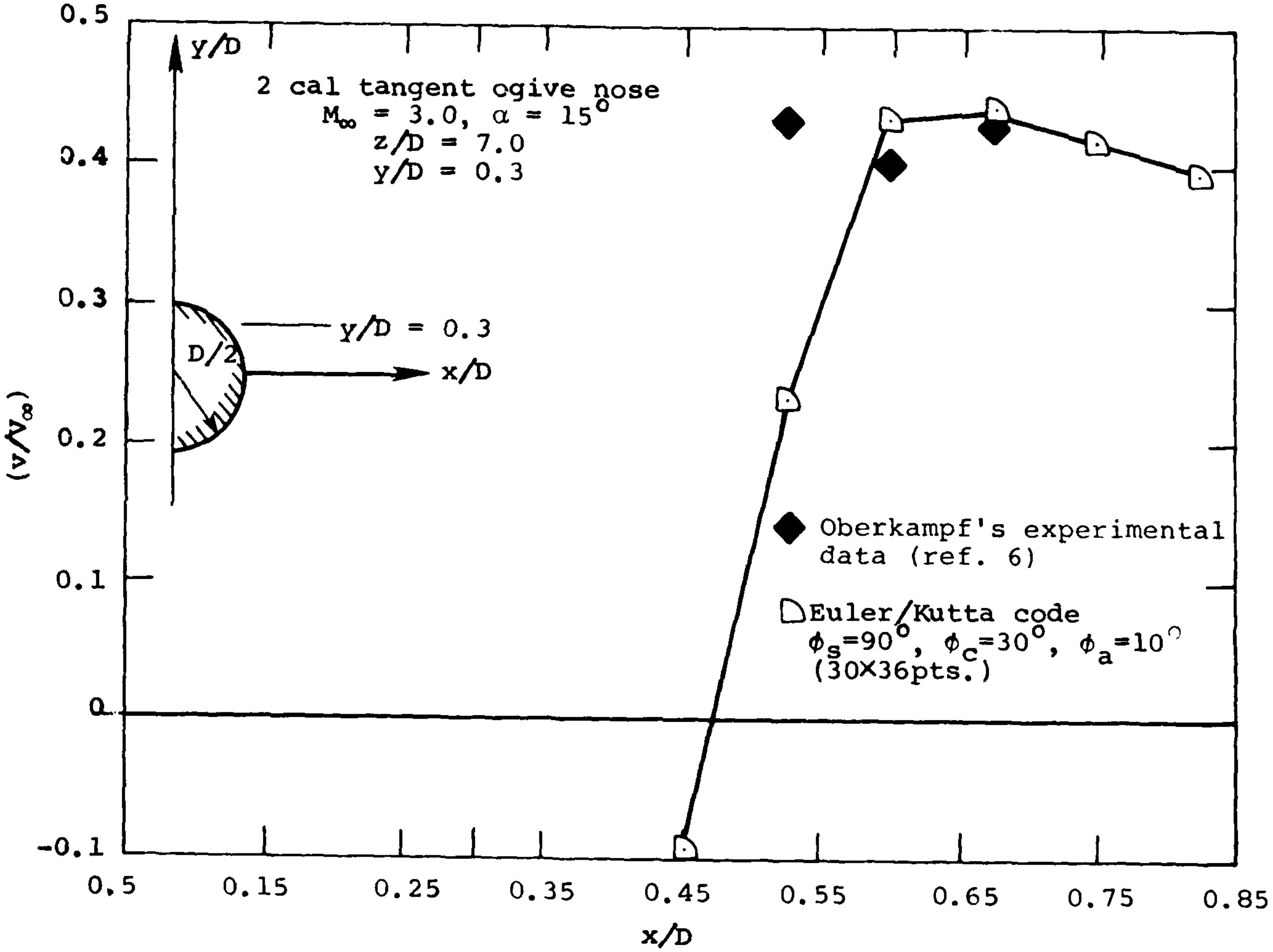

(a) z/D = 2.0

Figure 25.- Vertical velocity component vs. x/D at Y/D = 0.3.

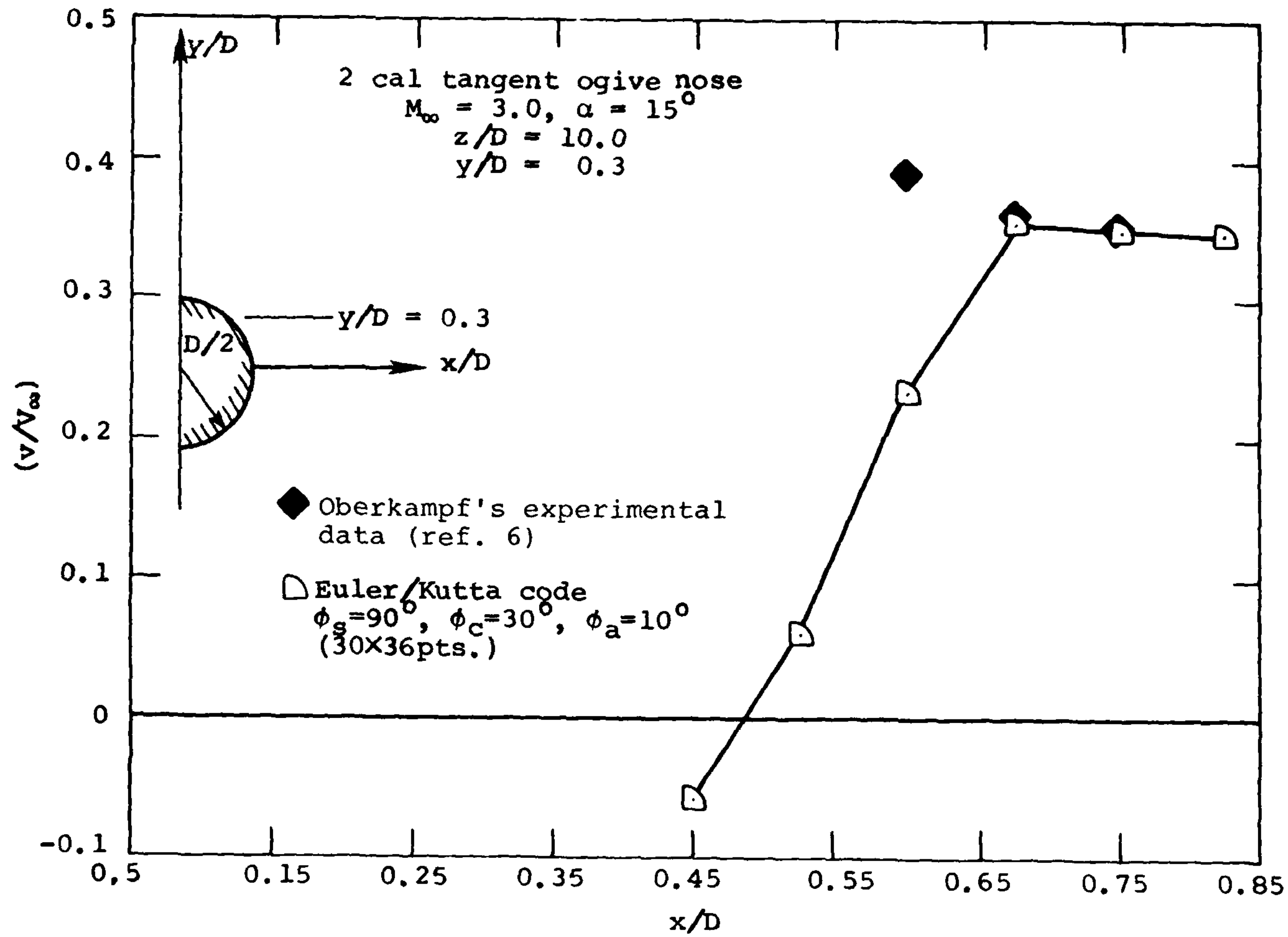

(b) z/D = 10.0

Figure 25.- Continued.

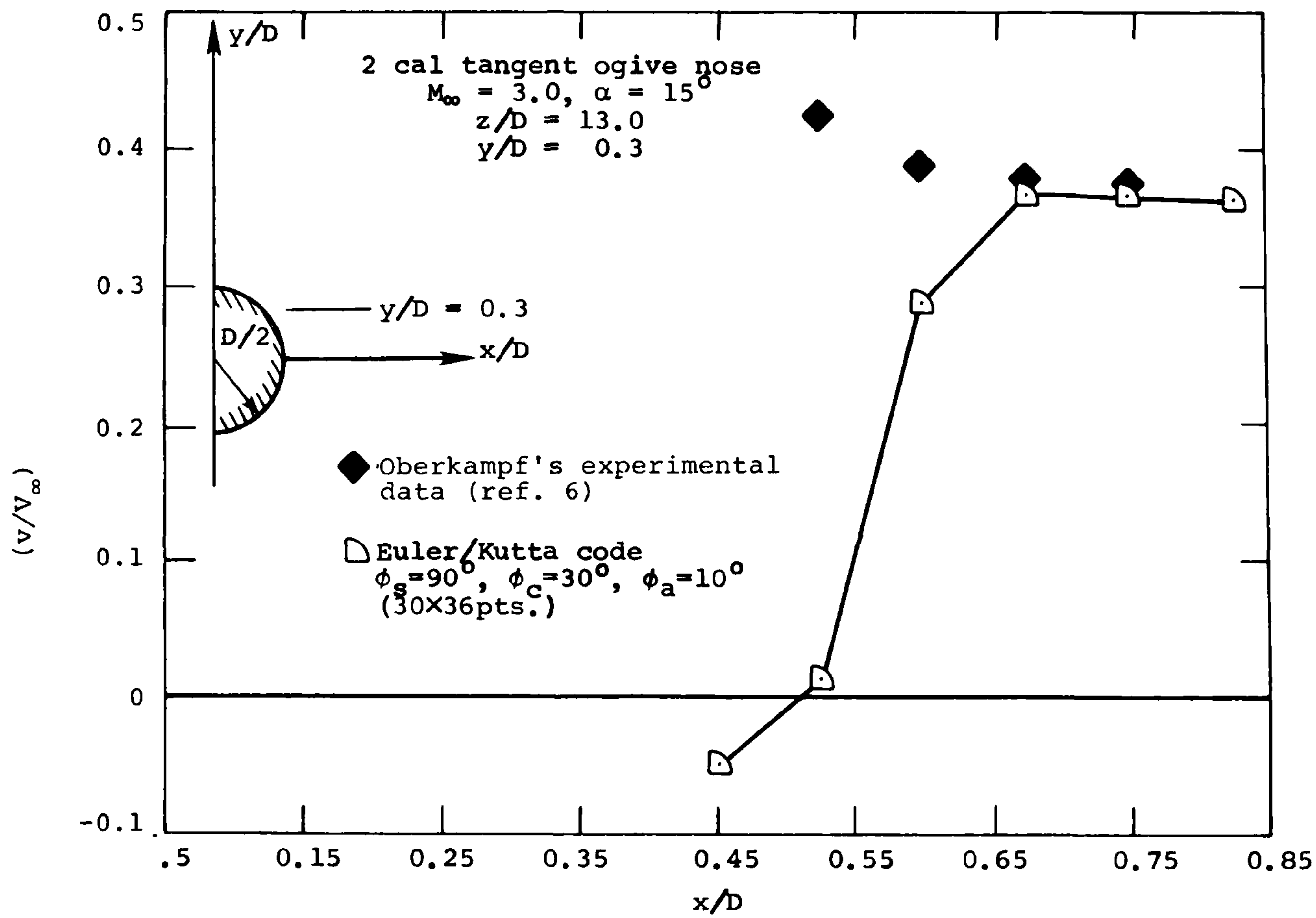

(c) z/D = 13.0

Figure 25.- Concluded.

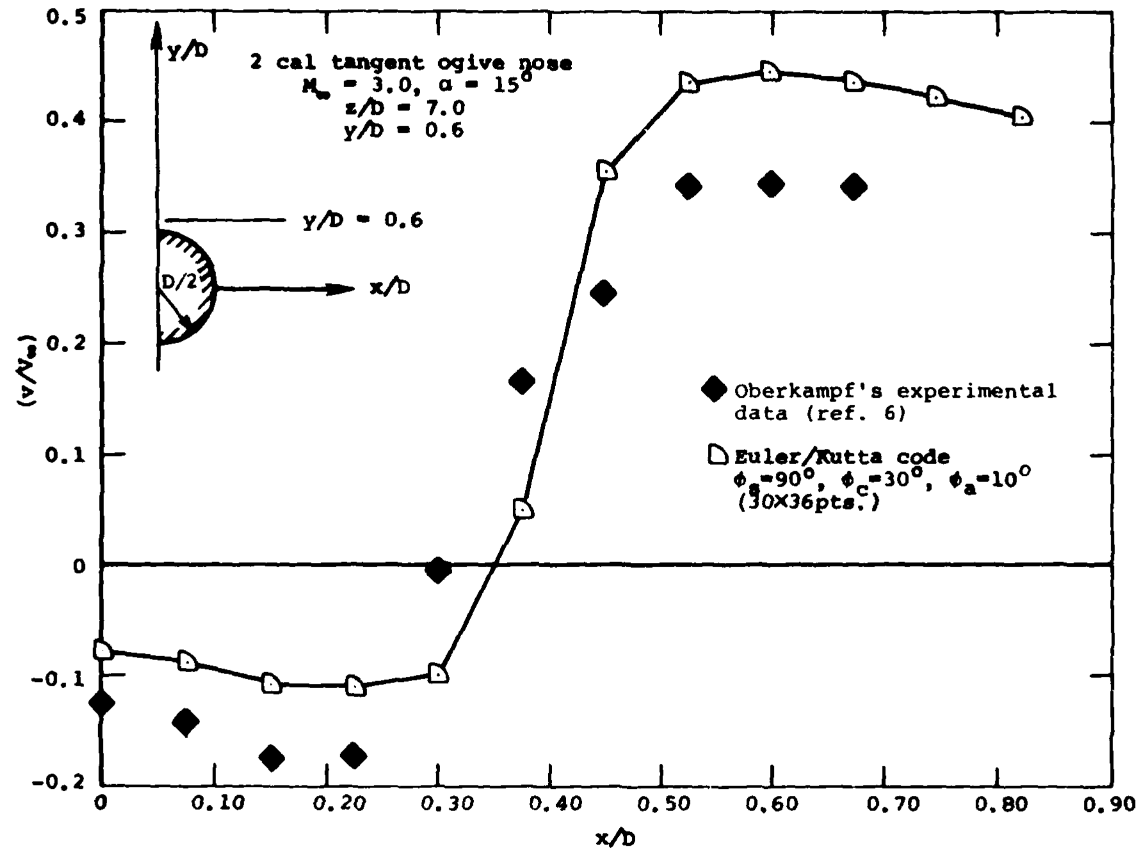

(a) z/D = 7.0

Figure 26.- Vertical velocity component vs. x/D at y/D = 0.6.

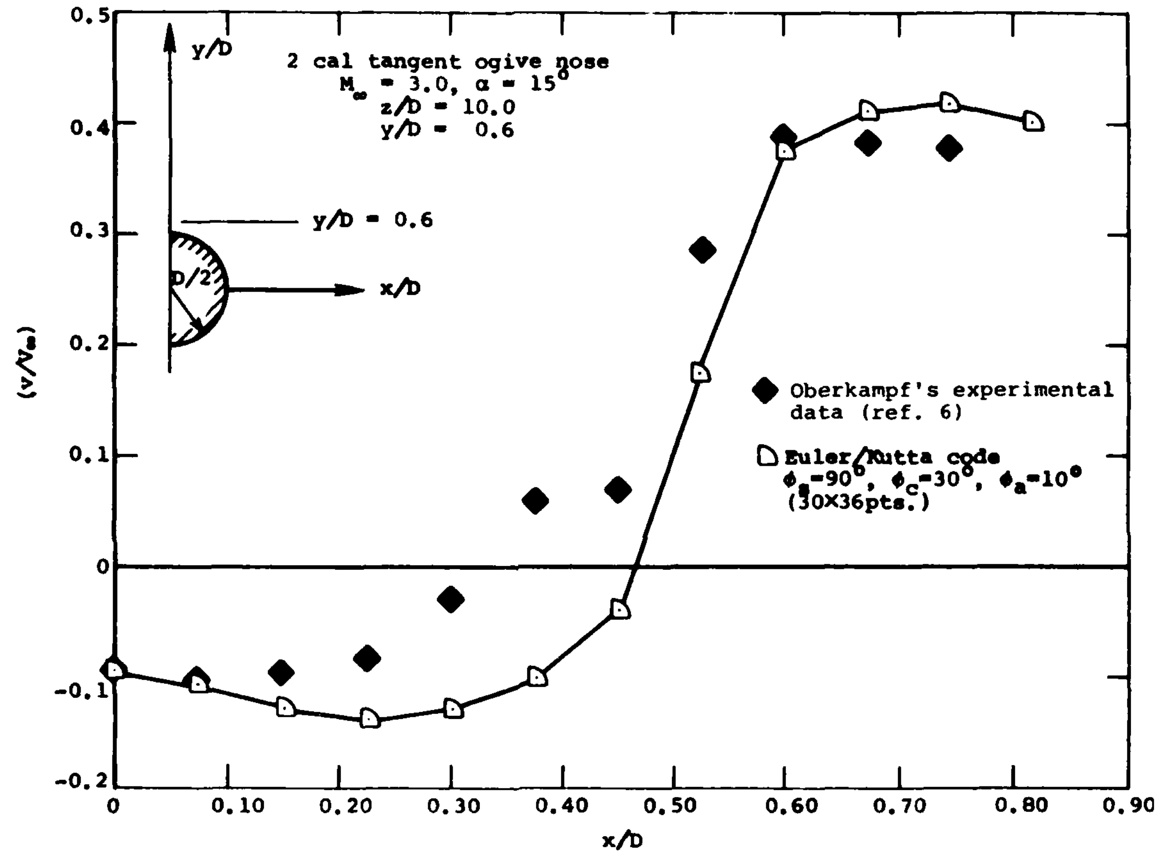

(b) z/D = 10.0

Figure 26.- Continued.

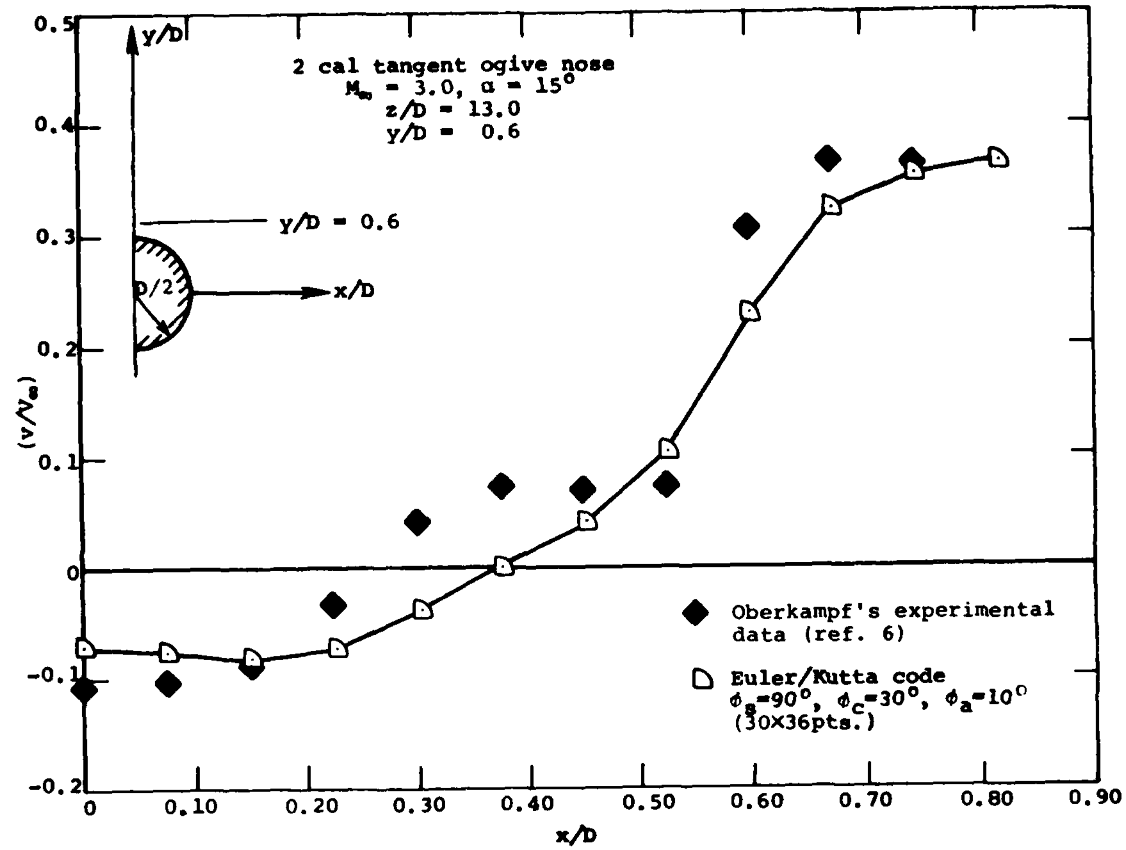

(c) z/D = 13.0

Figure 26.- Concluded.

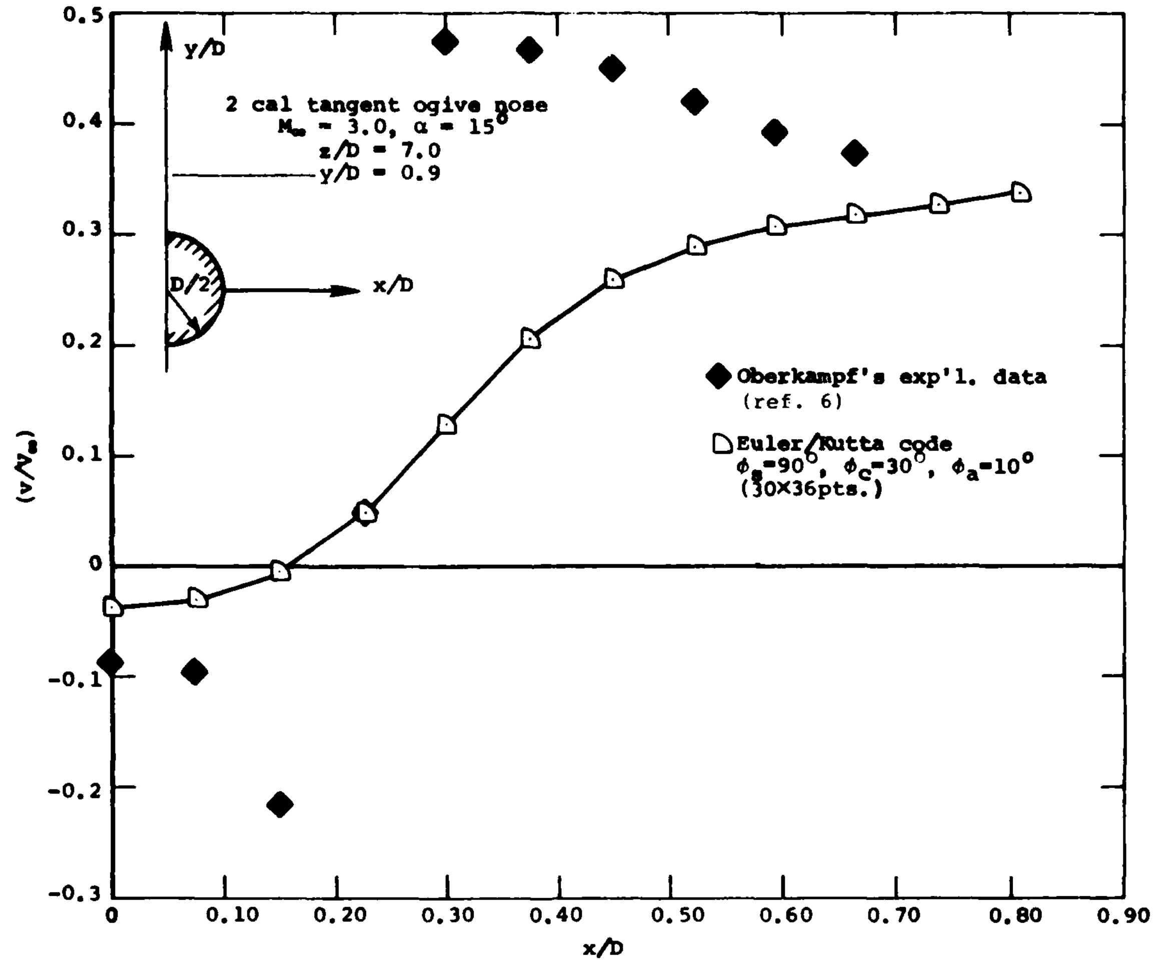

(a) z/D = 7.0

Figure 27.- Vertical velocity component vs. x/D at y/D = 0.9.

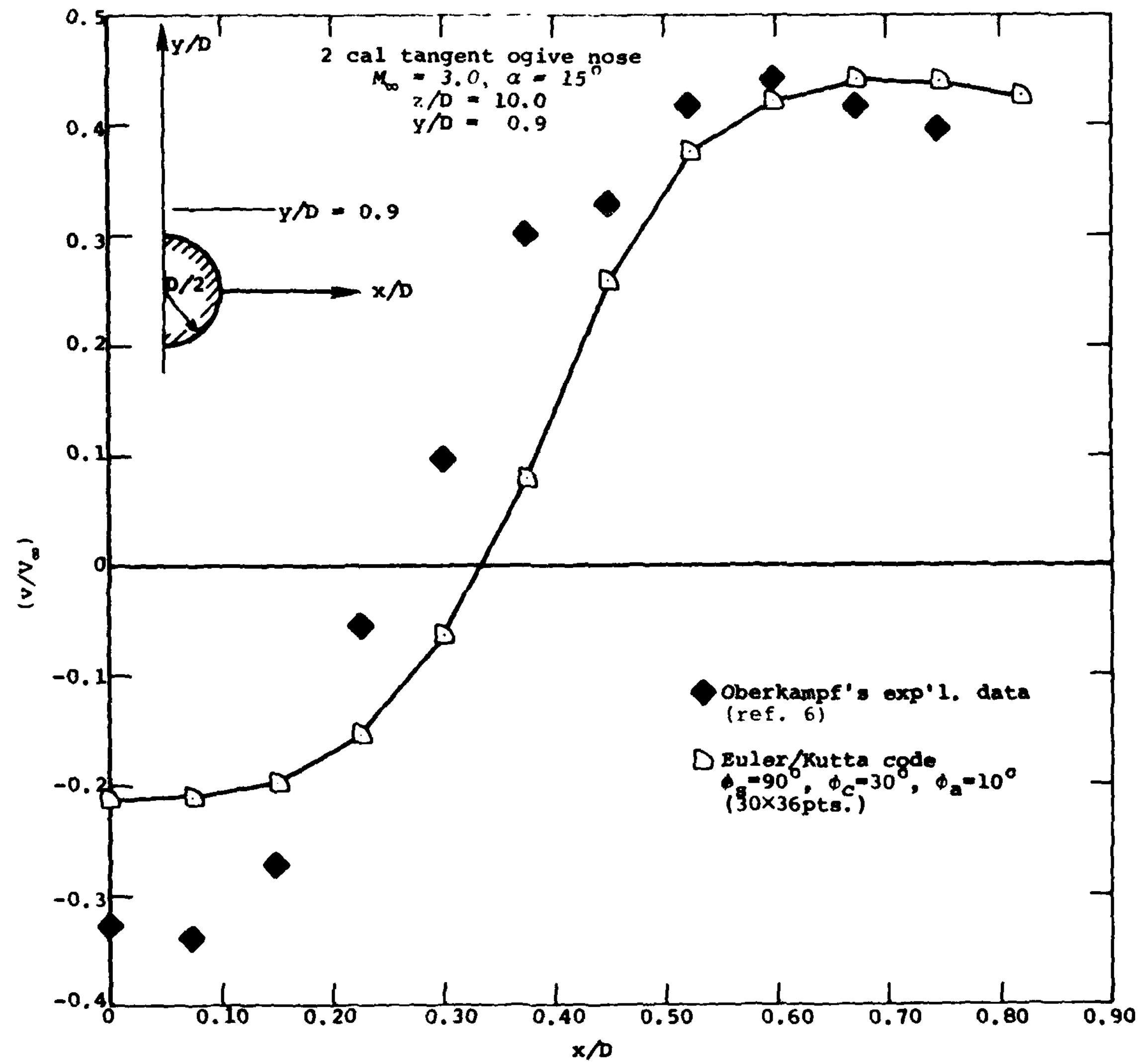

(b) z/D = 10.0

Figure 27.- Continued.

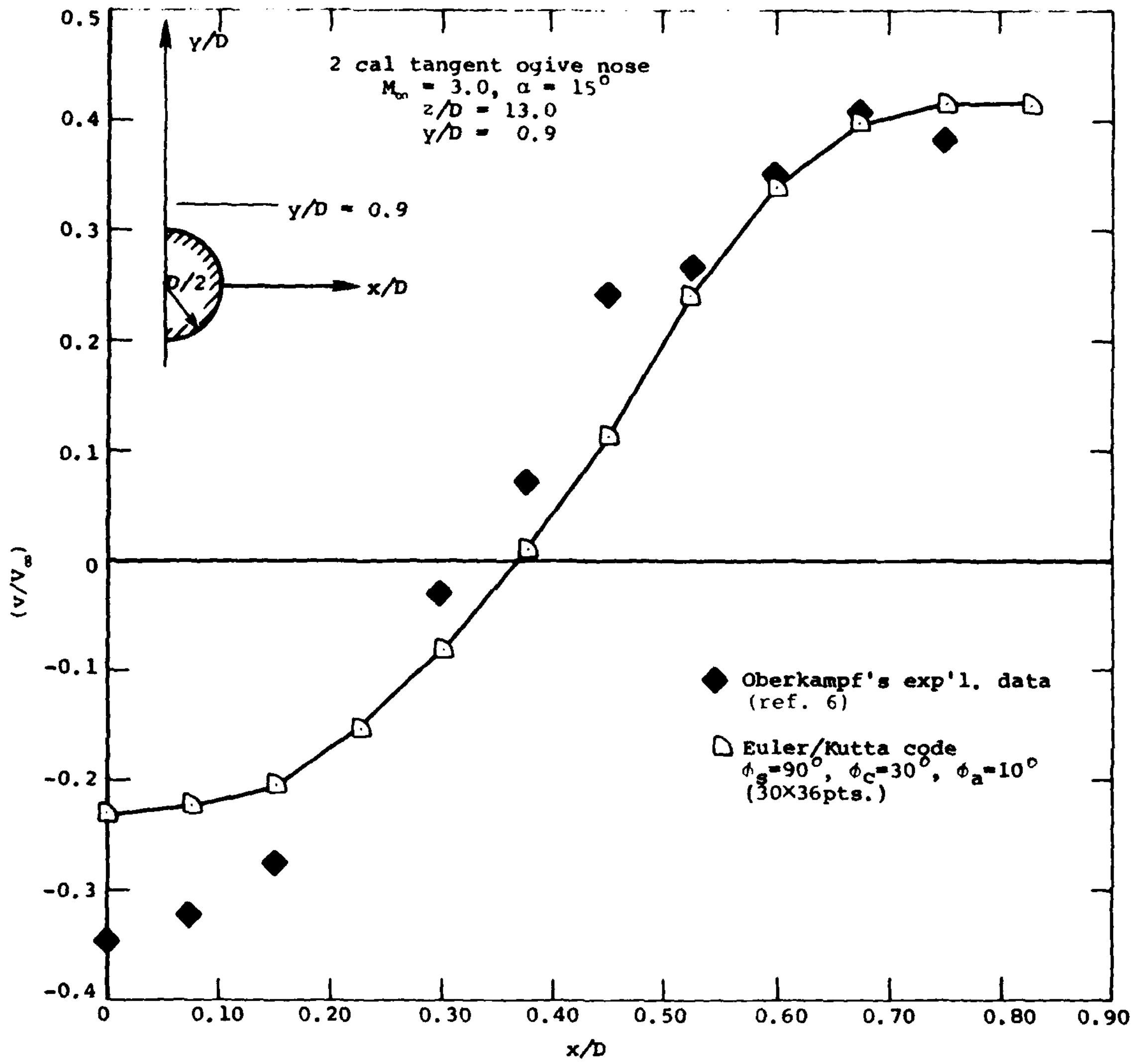

(c) z/D = 13.0

Figure 27.- Concluded.

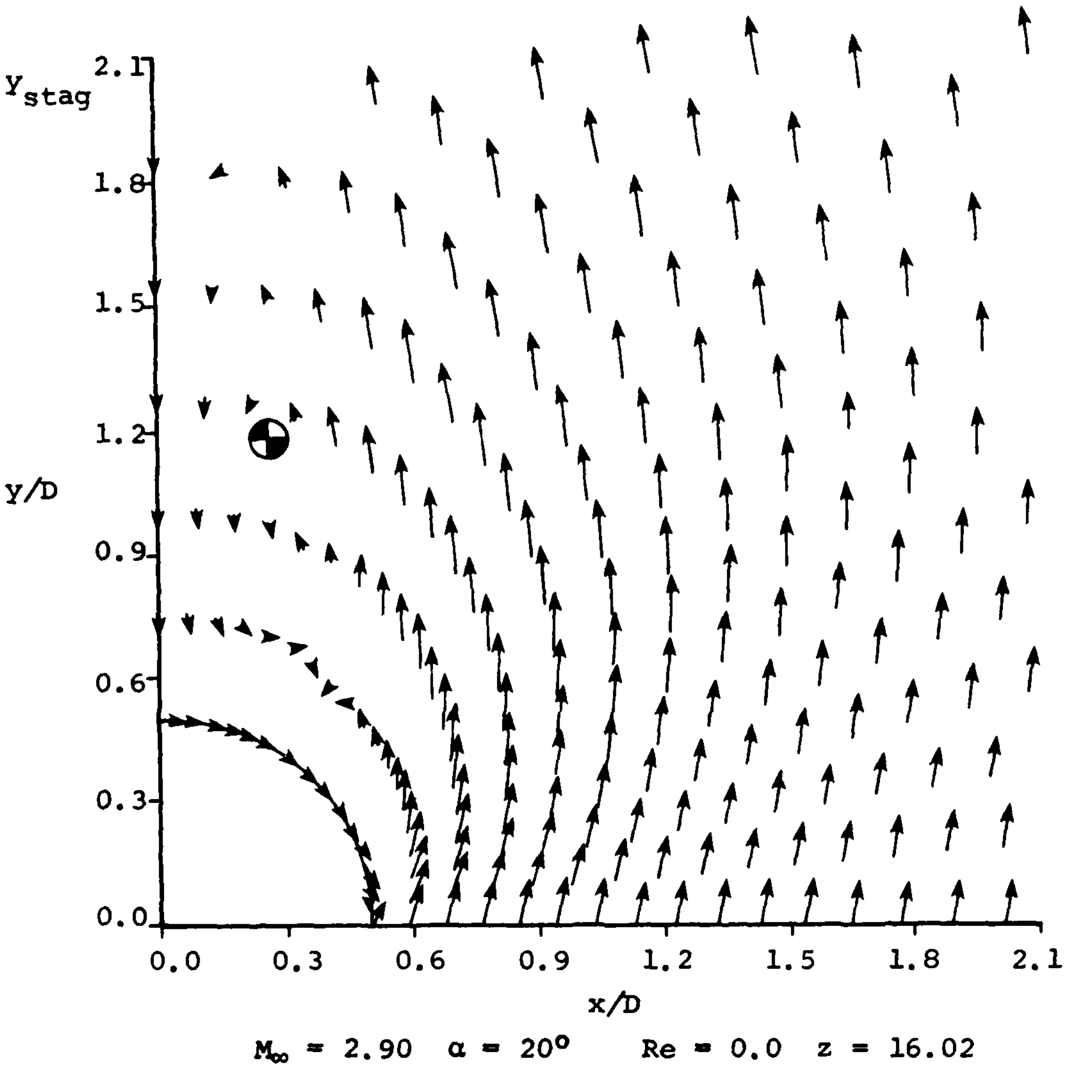

(a) Euler/Kutta code

Figure 28.- Numerical results of cross flow velocity vectors for 5 caliber tangent-ogive cylinder at z/D = 16 calibers for M_∞ = 2.90 and α = 20°.

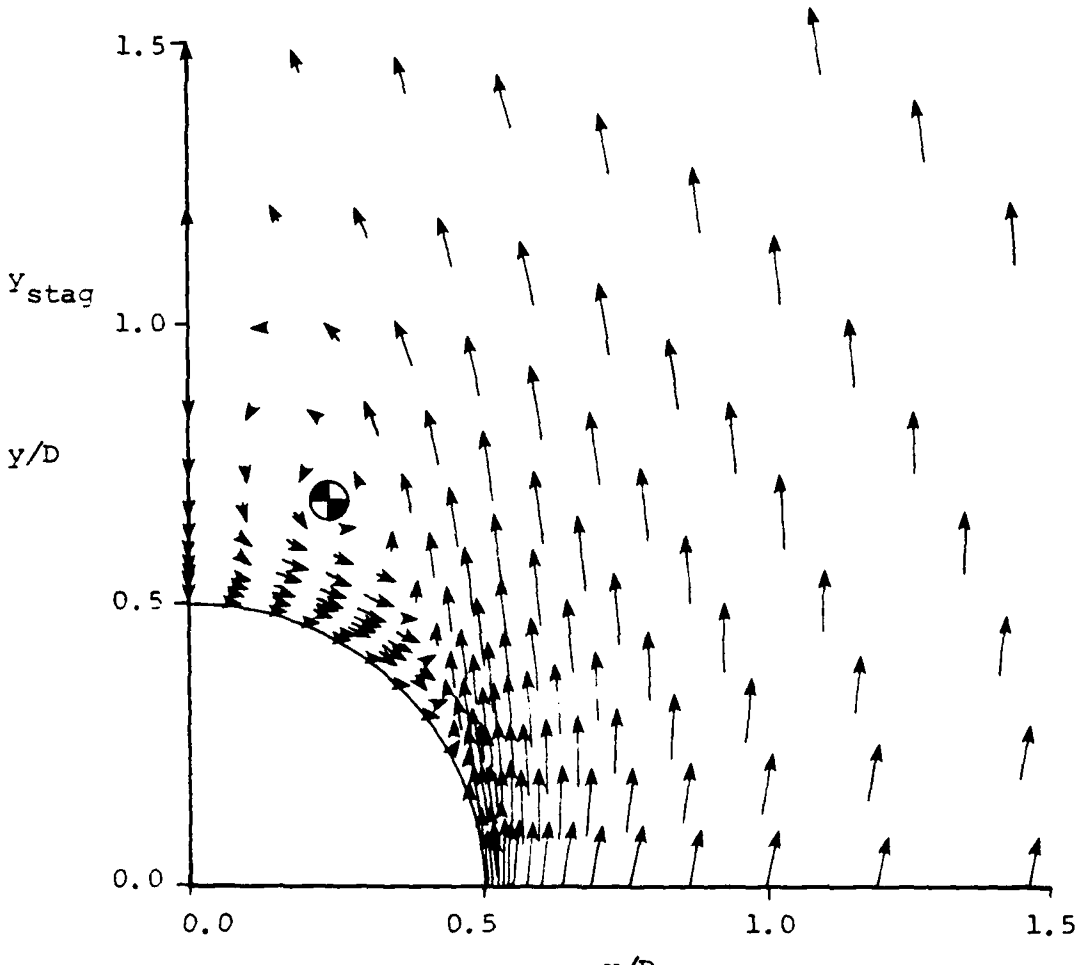

$M_\infty = 2.90 \quad \alpha = 20^{\circ} \quad Re = 1.2\times10^{5}$

(b) Parabolized Navier-Stokes code (Pulliam-ref. 18)

Figure 28.- Concluded.

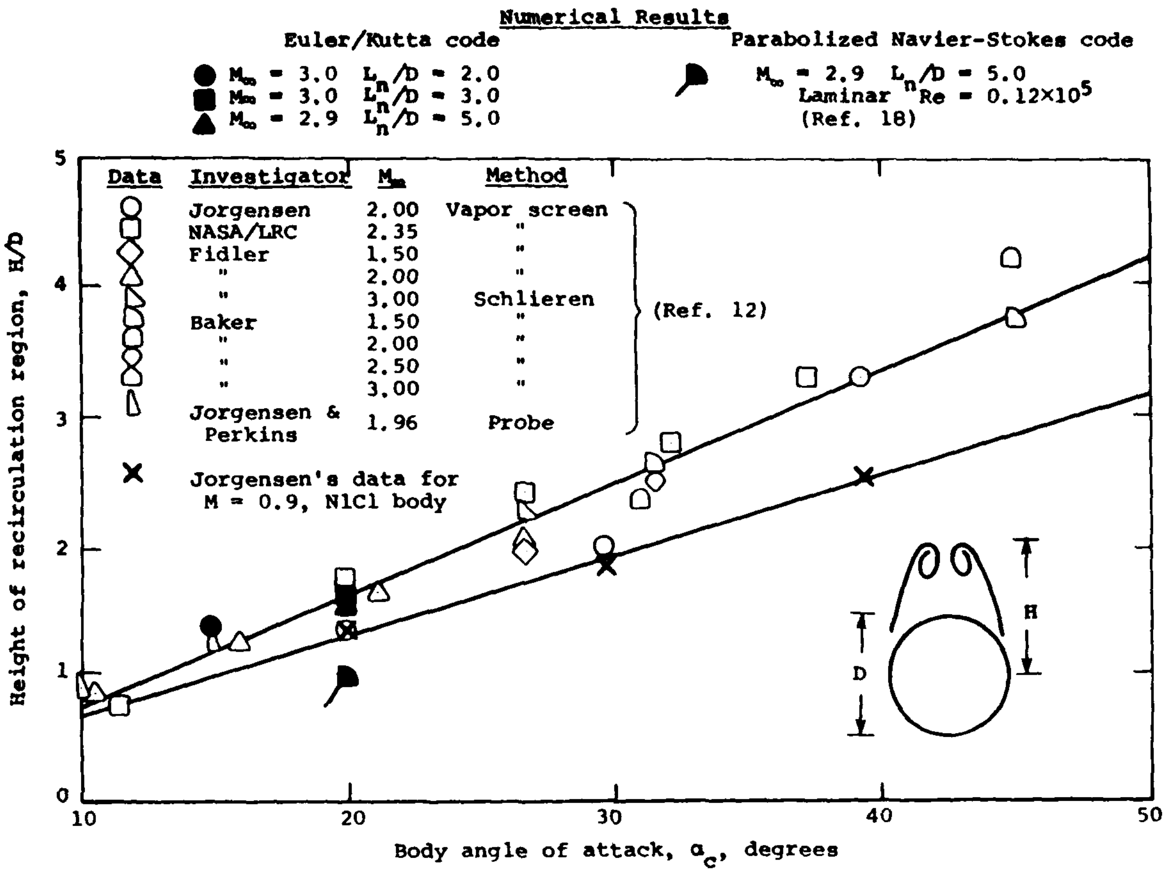

Figure 29.- Estimated height of top of recirculation region at z/D = 10 for tangent-ogive cylinder.

DISTRIBUTION LIST

Technical Library
Building 313
Ballistic Research Laboratories
Aberdeen Proving Ground, MD 21005

Mr. Aviars Celmins
Ballistic Research Laboratory
Ballistic Modelling Division
Aberdeen Proving Ground, MD 21005

Dr. P. J. Roache
Ecodynamics Research Associates, Inc.
P. O. Box 8172
Albuquerque, NM 87108

Defense Technical Information Center
Cameron Station, Building 5
Alexandria, VA 22314 (12)

Library
Naval Academy
Annapolis, MD 21402

Director, Tactical Technology Office
Defense Advanced Research Projects Agency
1400 Wilson Blvd.
Arlington, VA 22209

Code 200B
Office of Naval Research
800 N. Quincy Street
Arlington, VA 22217

Code 438
Office of Naval Research
800 N. Quincy Street
Arlington, VA 22217 (2)

Dr. J. L. Potter
Deputy Director, Technology
von Karman Gas Dynamics Facility
Arnold Air Force Station, TN 37389

Professor J. C. Wu
School of Aerospace Engineering
Georgia Institute of Technology
Atlanta, GA 30332

Library
Aerojet-General Corporation
6352 North Irwindale Avenue
Azusa, CA 91702

NASA Scientific and Technical Information Facility
P. O. Box 8757
Baltimore/Washington International Airport, MD 21240

Dr. K. C. Wang
College of Engineering
San Diego State University
San Diego, CA 92182

Professor A. J. Chorin
Department of Mathematics
University of California
Berkeley, CA 94720

Professor M. Holt
Department of Mechanical Engineering
University of California
Berkeley, CA 94720

Dr. H. R. Chaplin
Code 1600
David W. Taylor Naval Ship Research and Development Center
Bethesda, MD 20084

Dr. Hans Lugt
Code 1802
David W. Taylor Naval Ship Research and Development Center
Bethesda, MD 20084

Dr. Francois Frenkiel
Code 1802
David W. Taylor Naval Ship Research and Development Center
Bethesda, MD 20084

Dr. T. C. Tai
Code 1606
David W. Taylor Naval Ship Research and Development Center
Bethesda, MD 20084

DISTRIBUTION LIST (Continued)

Dr. G. R. Inger
Dept. of Aerospace Engineering
Virginia Polytechnic Institute and
State University
Blacksburg, VA 24061

Professor C. H. Lewis
Dept. of Aerospace and Ocean Engrg.
Virginia Polytechnic Institute and
State University
Blacksburg, VA 24061

Professor A. H. Nayfeh
Dept. of Engineering Science
Virginia Polytechnic Institute and
State University
Blacksburg, VA 24061

Dr. A. Rubel
Research Department
Grumman Aerospace Corporation
Bethpage, NY 11714

Commanding Officer
Office of Naval Research
Eastern/Central Regional Office
666 Summer St., Bldg. 114, Section D
Boston, MA 02210

Dr. J. C. Erickson, Jr.
CALSPAN Corporation
Advanced Technology Center
P. O. Box 400
Buffalo, NY 14225

Dr. T. J. Falk
CALSPAN Corporation
Advanced Technology Center
P. O. Box 400
Buffalo, NY 14225

Dr. C. Witliff
CALSPAN Corporation
Advanced Technology Center
P. O. Box 400
Buffalo, NY 14225

Prof. R. F. Probstein
Dept. of Mechanical Engineering
Massachusetts Institute of Technology
Cambridge, MA 02139

Commanding Officer
Office of Naval Research Branch Office
536 South Clark Street
Chicago, IL 60605

Code 753
Naval Weapons Center
China Lake, CA 93555

Mr. J. Marshall
Code 4063
Naval Weapons Center
China Lake, CA 93555

Professor R. T. Davis
Dept. of Aerospace Engineering
University of Cincinnati
Cincinnati, OH 45221

Professor S. G. Rubin
Dept. of Aerospace Engineering and
Applied Mechanics
University of Cincinnati
Cincinnati, OH 45221

Library MS 60-3
NASA Lewis Research Center
21000 Brookpark Road
Cleveland, OH 44135

Dr. J. D. Anderson, Jr.
Chairman, Dept. of Aerospace Engrg.
College of Engineering
University of Maryland
College Park, MD 20742

Professor O. Burggraf
Dept. of Aeronautical and Astro-
nautical Engineering
Ohio State University
1314 Kinnear Road
Columbus, OH 43212

DISTRIBUTION LIST (Continued)

Technical Library
Naval Surface Weapons Center
Dahlgren Laboratory
Dahlgren, VA 22448

Dr. F. Moore
Naval Surface Weapons Center
Dahlgren Laboratory
Dahlgren, VA 22448

Technical Library 2-51131
LTV Aerospace Corporation
P. O. Box 5907
Dallas, TX 75222

Library, United Aircraft Corporation
Research Laboratories
Silver Lane
East Hartford, CT 06108

Professor G. Moretti
Polytechnic Institute of New York
Long Island Center
Dept. of Aerospace Engrg. and
Applied Mechanics
Route 110
Farmingdale, NY 11735

Dr. W. R. Briley
Scientific Research Associates, Inc.
P. O. Box 498
Glastonbury, CT 06033

Professor P. Gordon
Calumet Campus
Dept. of Mathematics
Purdue University
Hammond, IN 46323

Library (MS 185)
NASA Langley Research Center
Langley Station
Hampton, VA 23665

Professor A. Chapmann
Chairman, Mechanical Engineering Dept.
William M. Rice Institute
Box 1892
Houston, TX 77001

Technical Library
Naval Ordnance Station
Indian Head, MD 20640

Professor D. A. Caughey
Sibley School of Mechanical and
Aerospace Engineering
Cornell University
Ithaca, NY 14850

Professor E. L. Resler
Sibley School of Mechanical and
Aerospace Engineering
Cornell University
Ithaca, NY 14850

Professor S. F. Shen
Sibley School of Mechanical and
Aerospace Engineering
Cornell University
Ithaca, NY 14850

Library
Midwest Research Institute
425 Volker Boulevard
Kansas City, MO 64110

Dr. M. M. Hafez
Flow Research, Inc.
P. O. Box 5040
Kent, WA 98031

Dr. E. M. Murman
Flow Research, Inc.
P. O. Box 5040
Kent, WA 98031

Dr. J. J. Riley
Flow Research, Inc.
P. O. Box 5040
Kent, WA 98031

Dr. S. A. Orszag
Cambridge Hydrodynamics, Inc.
54 Baskin Road
Lexington, MA 02173

Dr. P. Bradshaw
Imperial College of Science and Technology
Department of Aeronautics
Prince Consort Road
London SW7 2BY, England

Professor T. Cebeci
Mechanical Engineering Department
California State University, Long Beach
Long Beach, CA 90840

Dr. H. K. Cheng
University of Souther California
Department of Aerospace Engrg.
University Park
Los Angeles, CA 90007

Professor J. D. Cole
Mechanics and Structures Department
School of Engineering and Applied Science
University of California
Los Angeles, CA 90024

Engineering Library
University of Southern California
Box 77929
Los Angeles, CA 90007

Dr. C. -M. Ho
Dept. of Aerospace Engineering
University of Southern California
University Park
Los Angeles, CA 90007

Commanding Officer
Naval Ordnance Station
Louisville, KY 40214

Mr. B. H. Little, Jr.
Lockheed-Georgia Company
Department 72-74, Zone 369
Marietta, GA 30061

Professor E. R. G. Eckert
University of Minnesota
241 Mechanical Engineering Bldg.
Minneapolis, MN 55455

Dr. Gary Chapman
Mail Stop 227-4
Ames Research Center
Moffett Field, CA 94035

Library
Naval Postgraduate School
Monterey, CA 93940

Dr. J. L. Steger
Dept. of Aeronautics and Astronautics
Durand Building
Stanford University
Stanford, CA 94305

Dr. S. S. Stahara
Nielsen Engineering & Research, Inc.
510 Clyde Avenue
Mountain View, CA 94043

Engineering Societies Library
345 East 47th Street
New York, NY 10017

Professor A. Jameson
Mechanical and Aeronautical Engrg. Dept.
Princeton University
E Quad
Princeton, NJ 08540

DISTRIBUTION LIST (Continued)

Professor G. Miller
Dept. of Applied Science
New York University
26-36 Stuyvesant Street
New York, NY 10003

Office of Naval Research
New York Area Office
715 Broadway - 5th Floor
New York, NY 10003

Dr. A. Vaglio-Laurin
Dept. of Applied Science
New York University
26-36 Stuyvesant Street
New York, NY 10003

Mr. D. Farmer
Naval Ocean Research and Development Activity
Code 332
NSTL Station, MS 39522

Librarian, Aeronautical Library
National Research Council
Montreal Road
Ottawa 7, Canada

Lockheed Missiles and Space Company
Technical Information Center
3251 Hanover Street
Palo Alto, CA 94304

Commanding Officer
Office of Naval Research Western Regional Office
1030 East Green Street
Pasadena, CA 91106

Engineering Division
California Institute of Technology
Pasadena, CA 91109

Library
Jet Propulsion Laboratory
4800 Oak Grove Drive
Pasadena, CA 91103

Professor H. Liepmann
Department of Aeronautics
California Institute of Technology
Pasadena, CA 91109

Mr. L. I. Chasen, MGR-MSD Lib.
General Electric Company
Missile and Space Division
P. O. Box 8555
Philadelphia, PA 19101

Technical Library
Naval Missile Center
Point Mugu, CA 93042

Professor S. Bogdonoff
Gas Dynamics Laboratory
Dept. of Aerospace & Mechanical Sci.
Princeton University
Princeton, NJ 08540

Professor S. I. Cheng
Dept. of Aerospace & Mechanical Sci.
Princeton University
Princeton, NJ 08540

Dr. J. E. Yates
Aeronautical Research Associates of Princeton, Inc.
50 Washington Road
Princeton, NJ 08540

Professor L. Sirovich
Division of Applied Mathematics
Brown University
Providence, RI 02912

Redstone Scientific Information Center
Chief, Document Section
Army Missile Command
Redstone Arsenal, AL 35809

U.S. Army Research Office
P. O. Box 12211
Research Triangle Park, NC 27709

DISTRIBUTION LIST (Continued)

Editor, Applied Mechanics Review
Southwest Research Institute
8500 Culebra Road
San Antonio, TX 78228

Library and Information Services
General Dynamics-CONVAIR
P. O. Box 1128
San Diego, CA 92112

Dr. R. Magnus
General Dynamics-CONVAIR
Kearny Mesa Plant
P. O. Box 80847
San Diego, CA 92138

Office of Naval Research
San Francisco Area Office
One Hallidie Plaza, Suite 601
San Francisco, CA 94102

Library
The RAND Corporation
1700 Main Street
Santa Monica, CA 90401

Dr. P. E. Rubbert
Boeing Aerospace Company
Boeing Military Airplane Development Organization
P. O. Box 3707
Seattle, WA 98124

Dr. H. Yoshihara
Boeing Aerospace Company
P. O. Box 3999
Mail Stop 41-18
Seattle, WA 98124

Librarian
Naval Surface Weapons Center
White Oak Laboratory
Silver Spring, MD 20910

Dr. J. M. Solomon
Naval Surface Weapons Center
White Oak Laboratory
Silver Spring, MD 20910

Professor J. H. Ferziger
Dept. of Mechanical Engineering
Stanford University
Stanford, CA 94305

Professor K. Karamcheti
Dept. of Aeronautics and Astronautics
Stanford University
Stanford, CA 94305

Professor O. Bunemann
Institute for Plasma Research
Stanford University
Stanford, CA 94305

Engineering Library
McDonnell Douglas Corporation
Department 218, Building 101
P. O. Box 516
St. Louis, MO 63166

Dr. R. J. Hakkinen
McDonnell Douglas Corporation
Department 222
P. O. Box 516
St. Louis, MO 63166

Dr. N. Malmuth
Rockwell International Science Center
1049 Camino Dos Rios
P. O. Box 1085
Thousand Oaks, CA 91360

Library
Institute of Aerospace Studies
University of Toronto
Toronto 5, Canada

Professor W. R. Sears
Aerospace and Mechanical Engineering
University of Arizona
Tucson, AZ 95721

Professor A. R. Seebass
Dept. of Aerospace and Mechanical Engineering
University of Arizona
Tucson, AZ 95721

DISTRIBUTION LIST (Concluded)

Dr. K. T. Yen
Code 3015
Naval Air Development Center
Warminster, PA 18974

Air Force Office of Scientific
Research (SREM)
Building 410, Bolling AFB
Washington, DC 20332

Chief of Research and Development
Office of Chief of Staff
Department of the Army
Washington, DC 20310

Library of Congress
Science and Technology Division
Washington, DC 20540

Director of Research (Code RR)
National Aeronautics and Space
Administration
600 Independence Avenue, SW
Washington, DC 20546

Library
National Bureau of Standards
Washington, DC 20234

National Science Foundation
Engineering Division
1800 G Street, NW
Washington, DC 20550

AIR 320D
Naval Air Systems Command
Washington, DC 20361

AIR 950D
Naval Air Systems Command
Washington, DC 20375

Code 2627
Naval Research Laboratory
Washington, DC 20375

SEA 03512
Naval Sea Systems Command
Washington, DC 20362

Phillip J. Andrews
SEA 61R2
Naval Sea Systems Command
Washington, DC 20362

Dr. Charles Watkins
Head, Mechanical Engineering Dept.
Howard University
Washington, DC 20059

Dr. A. L. Slafkosky
Scientific Advisor
Commandant of the Marine Corps (Code AX)
Washington, DC 20380

Director
Weapons Systems Evaluation Group
Washington, DC 20350

Research Library
AVCO Corporation
Missile Systems Division
201 Lowel Street
Wilmington, MA 01887

AFAPL (APRC)
AB
Wright Patterson AFB, OH 45433

Dr. Donald J. Harney
AFFDL/FX
Wright Patterson AFB, OH 45433

Flow Research
1320 Fenwick Lane
Suite 401
Silver Spring, MD 20910